

1 Upper ocean temperature characteristics in the subantarctic 2 Southeast Pacific based on biomarker reconstructions

3 Julia R. Hagemann¹, Lester Lembke-Jene¹, Frank Lamy¹, Maria-Elena Vorrath², Jérôme Kaiser³, Juliane
4 Müller¹, Helge W. Arz³, Jens Hefter¹, Andrea Jaeschke⁴, Nicoletta Ruggieri¹, Ralf Tiedemann¹

5 ¹Alfred Wegener Institute, Helmholtz Centre for Polar and Marine Research, 27570 Bremerhaven, Germany

6 ²Institute for Geology, University Hamburg, 20146 Hamburg, Germany

7 ³Leibniz-Institute for Baltic Sea Research Warnemünde, 18119 Rostock, Germany

8 ⁴Institute of Geology and Mineralogy, University of Cologne, 50923 Cologne, Germany

9
10 Correspondence to: Julia. R. Hagemann (Julia.Hagemann@awi.de) and Lester Lembke-Jene (Lester.Lembke-Jene@awi.de)

11 **Abstract.** Alkenones and **isoprenoid** Glycerol Dialkyl Glycerol Tetraether lipids (**isoGDGT**) as remnants of living organisms
12 are widely used biomarkers for determining past oceans' water temperatures. The organisms these proxy carriers stem from,
13 are influenced by a number of environmental parameters, such as water depth, nutrient availability, light conditions or
14 seasonality, which all may significantly bias the calibration to ambient water temperatures. Reliable temperature
15 determinations remain thus challenging, especially in higher latitudes and for under-sampled regions. We analyzed 33 sediment
16 surface samples from the Southern Chilean continental margin and the Drake Passage for alkenones and **isoGDGTs** and
17 compared the results with gridded instrumental reference data from the World Ocean Atlas 2005 (WOA05), as well as
18 previously published data from an extended study area covering the Central and Western South Pacific towards the New
19 Zealand continental margin. We show that for alkenone-derived **Sea Surface Temperatures (SST)**, the widely-used global core-
20 top calibration of Müller et al. (1998) yields the smallest **deviation of the WOA05-based SSTs**. The calibration of Sikes et al.
21 (1997) **instead**, adapted to higher latitudes and supposed to show summer SSTs, overestimates modern WOA05-based SSTs.
22 Our alkenone SSTs show a slight seasonal shift of ~1° C at the Southern Chilean Margin and up to ~2° C in the Drake Passage
23 towards austral summer SSTs. **Samples in the Central South Pacific on the other hand** reflect an annual mean signal. We show
24 that for **isoGDGT-based temperatures** **the subsurface calibration of Kim et al. (2012a) best reflects temperatures from the**
25 **WOA05** in areas north of the Subantarctic Front (SAF). Temperatures south of the SAF **in contrast** are significantly
26 overestimated by up to 14° C, irrespective of the applied calibration. **In addition, we used** the GDGT [2]/[3]-ratios, which **gives**
27 **an indication of the production depth of the isoGDGTs and/or potentially influences from land**. Our samples reflect a
28 subsurface (0 to 200 m water depth) rather than a surface (0 – 50 m water depth) signal **in the entire study area and show a**
29 **correlation with the monthly dust distribution in the South Pacific, indicating terrigenous influences**. The overestimation of
30 **isoGDGTs** surface and subsurface temperatures south of the SAF highlights the need for a re-assessment of existing
31 calibrations in the polar Southern Ocean. **Therefore, we suggest a modified Southern Ocean TEX¹₈₆ – based calibration for**

hat gelöscht: residuals

hat gelöscht: , whereas t

hat gelöscht: (summer and annual mean)

hat gelöscht: whereas s

hat gelöscht: , a more complex pattern emerges. I

hat gelöscht: the subsurface calibration of Kim et al. (2012a) best reflects temperatures from the WOA05, largely within the margin error of ±2.2° C...

hat gelöscht: instead

hat gelöscht: Based on a qualitative assessment of

hat gelöscht: likely indicate water depth of origin, o

hat gelöscht: , and leads to limitations in reliably both obtaining absolute values and assessing relative changes.

45 surface and subsurface temperatures, which shows a lower temperature sensitivity and yields principally lower absolute
46 temperatures, which align more closely with WOA05-derived values and also OH-isoGDGT-derived temperatures.

hat gelöscht: GDGT-based

hat gelöscht: of the TEX₈₆

47 1 Introduction

48 Alkenones (e.g., Brassell et al., 1986; Herbert, 2001, 2014) and isoGDGTs (isoprenoid Glycerol Dialkyl Glycerol Tetraether;
49 Schouten et al., 2002; Schouten et al., 2013a) are widely used for determining oceans' past water temperatures. These
50 biomarkers are present in all oceans and occur from the tropics to high latitudes (e.g., Herbert et al., 2010; Sikes et al., 1997;
51 Müller et al., 1998; Conte et al., 2006). Alkenone-derived sea surface temperatures (SSTs) are based on lipid remains of
52 photoautotrophic Coccolithophorids (e.g., Baumann et al., 2005; Brassell et al., 1986). The ratio of di- and tri-unsaturated
53 alkenones, expressed as the Unsaturation Ketone index U^K₃₇ (Table A1) is reflecting SSTs (Prah and Wakeham, 1987).
54 Calculation of SSTs is based on calibration equations developed over the past ~40 years (Table A1). Most of these empirically-
55 derived equations are relatively similar, and based on comparison of either culture experiments (Prah et al., 1988; Prah and
56 Wakeham, 1987) or surface sediment samples from tropical to subpolar regions with corresponding instrumental data (Müller
57 et al., 1998). Other calibrations (e.g., Sikes et al., 1997) were developed specifically for (sub)polar regions and are adapted for
58 a seasonal bias toward summer SSTs. Henceforth, we use the terms Müller98 for the calibration by Müller et al. (1998) and
59 Sikes97 for the calibration by Sikes et al. (1997; Table A1).

hat formatiert: Schriftart: Fett

hat formatiert: Schriftart: Fett

hat formatiert: Schriftart: Fett

hat formatiert: Schriftart: Fett

hat gelöscht: In the following

60 The accuracy of alkenone-based calibrations can be influenced by other environmental factors besides temperature, such
61 as light levels, changes in growth rate or nutrient availability, but none of these factors seems to have an appreciable effect on
62 the U^K₃₇ index (e.g., Caniupán et al., 2014; Epstein et al., 2001; Herbert, 2001; Müller et al., 1998; Popp et al., 1998). In
63 contrast, preferential degradation of the alkenone C_{37:3} in sediment under aerobic conditions may bias the U^K₃₇ signal towards
64 warmer SSTs (Prah et al., 2010). Seasonality often plays a significant role at high latitudes (e.g., Max et al., 2020; Prah et al.,
65 2010), due to primary production being more pronounced in the thermal summer season and annual temperature differences
66 that increases with increasing latitude. In our study region, samples from the Central South Pacific most likely represent either
67 summer temperatures (with the Sikes97 calibration) or an annual mean (Müller98 calibration; Jaeschke et al., 2017). Prah et
68 al. (2010), using samples from the Chilean continental slope, found a slight seasonal summer bias south of ~50° S. In contrast,
69 studies from the North Pacific show a seasonal signal towards late summer to autumn SSTs that differ from the annual mean
70 by up to 6° C (e.g., Max et al., 2020; Prah et al., 2010).

hat gelöscht: However,

hat gelöscht: in higher latitudes

hat gelöscht: combined with the principally wider spread in temperatures across the seasonal cycle

hat gelöscht: the case of

hat gelöscht: are

hat gelöscht: to

hat gelöscht: instead

hat gelöscht: In addition

hat gelöscht: alkenone temperatures in higher latitudes

hat gelöscht: , recording late summer to autumn SSTs instead

hat gelöscht: In addition to the alkenone-derived paleothermometer, other biomarkers also bear considerable and well-established potential to reconstruct past temperatures.

hat verschoben (Einfügung) [1]

hat gelöscht: and

hat gelöscht: four

hat gelöscht: (GDGT-0; GDGT-1; GDGT-2; GDGT-3; Crenarchaeol)...

hat nach oben verschoben [1]: increases with growth temperature (Schouten et al., 2002).

71 IsoGDGTs are lipid remains of *Thaumarchaeota* (formerly called Crenarchaeota Group I; Brochier-Armanet et al., 2008)
72 that include a certain number of moieties, which increases with growth temperature (Schouten et al., 2002). The lipids GDGT-
73 0; GDGT-1; GDGT-2; GDGT-3 contain zero to three cyclopentane moieties in their molecule structure, whereas Crenarchaeol
74 and its isomer Cren' feature four cyclopentane and one hexane moieties. These ring structures regulate membrane fluidity of
75 *Thaumarchaeota* and change as an adaption to their ambient temperature (Chong, 2010; Gabriel and Chong, 2000; Schouten
76 et al., 2002). The number of moieties Determination of isoGDGT-derived water temperatures is based on the Tetraether index

100 (TEX₈₆; Schouten et al., 2002), or their modifications TEX^H₈₆ and TEX^L₈₆ (**Table A1**), which have been determined for water
101 temperatures >15° C and <15° C, respectively (Kim et al., 2010). While TEX^H₈₆ is a logarithmic function of the original index,
102 TEX^L₈₆ omits the GDGT-3 from the denominator and removes the isomer Cren^{*} from the equation, due to a weaker correlation
103 to water temperatures in cold regions (Kim et al., 2010). In addition to cyclopentane moieties, three OH-isoGDGTs may also
104 contribute to ambient temperature adaption (OH-isoGDGT-0, OH-isoGDGT-1, and OH-isoGDGT-2). These OH-isoGDGTs
105 occur globally, but in higher amounts in the polar regions, as further adaption of the *Thaumarchaeota* to the cold environment
106 (Fietz et al., 2013; Huguet et al., 2013; Liu et al., 2020). OH-isoGDGTs are frequently so important in polar regions or during
107 glacial phases that it has been recommended to include them in temperature calibrations (Fietz et al., 2020; Fietz et al., 2016).
108 In contrast to photo-autotrophic coccolithophores, *Thaumarchaeota* occur throughout the water column (Karner et al., 2001),
109 which complicates the attribution of the reconstructed temperature signal to specific water depths. In general, it is assumed
110 that *Thaumarchaeota* predominantly reflect either a subsurface, i.e., seasonal mixed-layer temperature (T_{sub}; 0 – 200 m water
111 depth), or an SST signal (**Table A1**), because the grazing and repacking of isoGDGTs into fecal pellets occurs most effectively
112 within the photic zone (Wuchter et al., 2005). The GDGT [2]/[3]-ratio can be used to roughly determine the habitat depth of
113 the *Thaumarchaeota*, since it increases with increasing water depth (Dong et al., 2019; Hernández-Sánchez et al., 2014; Kim
114 et al., 2015; Kim et al., 2016; Schouten et al., 2012; Taylor et al., 2013). For the subpolar and polar Southern Ocean, in
115 particular the extensive SE Pacific sector, only little information exists to date about the applicability of these different
116 temperature proxies and their respective calibrations. In addition, systematic comparisons between alkenone and isoGDGT-
117 based temperature reconstructions based on surface sediments have thus far been limited (e.g., Jaeschke et al., 2017; Kaiser et
118 al., 2015). We use the terms SST^HKim and SST^LKim for the two global surface calibrations by Kim et al. (2010), Tsub^HKim
119 and Tsub^LKim for the two global subsurface calibrations by Kim et al. (2012a, 2012b) and SST^HKaiser and Tsub^HKaiser for
120 the local surface and subsurface calibration by Kaiser et al. (2015; **Table A1**).

121 In this study, we present a new set of 33 sediment surface samples located along the Southern Chilean Margin (SCM) and
122 the Drake Passage (DP; ~52 – 62° S) to determine upper ocean water temperatures based on alkenones (U^K₃₇) and isoGDGTs
123 (TEX^H₈₆ and TEX^L₈₆). We compare our regional results with previously published data from an extended, temperate to subpolar
124 South Pacific study area (**Figure 1**).

125 We assess the applicability of the Müller98 and Sikes97 calibrations with World Ocean Atlas (WOA05)-based temperatures
126 and investigate the influence of seasonality on alkenone-based temperature reconstructions. Furthermore, we compare the
127 isoGDGT-based indices TEX^H₈₆ and TEX^L₈₆ and their most common calibrations for SST and Tsub (**Table A1**) with WOA05-
128 based temperatures. Lastly, we check the potential influence of habitat depth on signal incorporation on the basis of the GDGT
129 [2]/[3]-ratio and propose a new calibration specifically for the polar Pacific sector of the Southern Ocean (SO) south of the
130 Subantarctic Front.

hat formatiert: Schriftart: Fett

hat formatiert: Schriftart: Fett

hat gelöscht: deletes

hat gelöscht: recorded

hat formatiert: Schriftart: Fett

hat formatiert: Schriftart: Fett

hat gelöscht: qualitatively

hat gelöscht: those

hat gelöscht: In the following, w

hat formatiert: Schriftart: Fett

hat formatiert: Schriftart: Fett

136 2 Study Area

137 Our study area comprises the subpolar and polar SE Pacific sector of the SO, including the Drake Passage (Figure 1). One
138 important characteristic of the SO is the eastward-flowing Antarctic Circumpolar Current (ACC), which is largely driven by
139 Southern Westerly Winds (SWW) and buoyancy forcing (Rintoul, 2018; Watson et al., 2015). The ACC flows unimpeded
140 around Antarctica, and is only slowed down by the South American continent (Orsi et al., 1995), where the northern branch of
141 the ACC bifurcates at ~40 – 45° S into the northward-flowing Peru-Chile Current (PCC) and the southward-flowing Cape
142 Horn Current (CHC; Strub et al., 1998). CHC and ACC jointly transport ca. 130 – 150 Sv of water (e.g., Koenig et al., 2014)
143 through the ~800 km wide Drake Passage into the Atlantic Ocean (Figure 1).

144 Several fronts within the ACC characterize the convergence of water masses that differ in temperature, salinity and nutrient
145 content (Orsi et al., 1995). The northern boundary of the ACC is defined by the Subtropical Front (STF; Orsi et al., 1995),
146 followed from north to south by the Subantarctic Front (SAF), the Polar Front (PF) and the Southern ACC Front (SACCF).
147 Apart from the STF, which is interrupted by the South American continent, all three fronts (SAF, PF and SACCF) pass through
148 the Drake Passage (Orsi et al., 1995; Figure 1). The zones between the fronts are defined as areas with differing temperature
149 and salinity characteristics, both decreasing with increasing latitude. The SAF marks the beginning of the Antarctic
150 Intermediate Water's (AAIW) northward descent to a depth of ~500 m. AAIW itself is associated with a salinity minimum of
151 <34 PSU. The PF, on the other hand, marks the northern temperature limit of the cold Antarctic surface water. The SACCF
152 instead has no distinct separating features in the surface water. The boundary, is here defined along the mesopelagic temperature
153 maximum of the upwelled Upper Circumpolar Deep Water (UCDW; Orsi et al., 1995 and references therein).

154 3 Material and Methods

155 A total amount of 33 Multi-Corer (MUC) samples (Table A2) along the Southern Chilean Margin and the Drake Passage were
156 analyzed for alkenones and isoGDGTs. The samples were collected during R/V Polarstern expedition PS97 in February-April
157 2016 (Lamy, 2016) along a latitudinal transect on the Southern Chilean Margin and through the Southern Ocean frontal system.

158 The MUC samples were stored deep-frozen immediately after sampling onboard and freeze-dried afterwards in the
159 laboratory. Extraction of the biomarkers was carried out with two different approaches. Between 3 and 5 g of ground surface
160 sediment (0 – 1 cm) from each site was extracted either by an accelerated Solvent Extraction (DIONEX ASE 350; Thermo
161 Scientific) with DCM:MeOH (9:1, v:v) for the samples of the Chilean margin (including three samples from the Drake Passage)
162 or in an ultrasonic bath with DCM:MeOH (2:1, v:v) for the samples of the Drake Passage. As internal standard, 100 µl each
163 of the *n*-alkane C₃₆ or 2-nonadecanone standard and C₄₆ were added before extraction. The two data sets were initially used to
164 address differing research objectives. The samples from the Chilean margin (including three DP samples) were primarily used
165 for extracting alkenones for SST. Previous works on the DP samples, on the other hand, focused on highly branched
166 isoprenoids (HBIs), sterols and isoGDGTs (Lamping et al., 2021; Vorrath et al., 2020), and were extracted using sonication as
167 a lower recovery of higher unsaturated HBIs is known when using the ASE method (Belt et al., 2014). In contrast, the TEX₈₆

hat gelöscht: here

hat formatiert: Schriftart: Fett

hat formatiert: Schriftart: Fett

hat verschoben (Einfügung) [6]

169 [index does not appear to be substantially affected by extraction techniques](#) (Schouten et al., 2013b). [The good agreement](#)
170 [between the three ASE extraction DP samples and the ultrasonic bath samples \(Figure 7D – F\) suggests that the two data sets](#)
171 [are comparable](#).

172 The bulk of the solvent was removed by rotary evaporation, under a nitrogen gas stream or in a Rocket Evaporator (Genevac
173 – SP Scientific). The different fractions were chromatographically separated using small glass columns filled with 5 cm of
174 activated silicagel. After adding the sample, the column was rinsed with 5 ml *n*-hexane, 5 ml or 8 ml *n*-hexane:DCM (1:1,
175 v:v), 5 ml DCM and 4 ml DCM:MeOH (1:1, v:v) to yield *n*-alkanes, alkenones and isoGDGTs, respectively. The samples
176 were dried again and transferred into 2 ml vials. [For the measurement, the alkenone fractions were diluted with 200 – 20 µl *n*-](#)
177 [hexane, the GDGT fraction was filtered first, and then diluted with 50 – 120 µl *n*-hexane:isopropanol \(99:1, v:v\).](#)

178 Alkenones were injected with 1 µl solvent and Helium as carrier gas into an Agilent HP6890 Gas Chromatograph equipped
179 with a 60 m DB-1 MS column and a flame ionization detector. The oven temperature was increased from initially 60° C to
180 150° C with 20° C min⁻¹ and thereafter with 6° C min⁻¹ until 320° C were reached.

181 For the GDGT [measurements of most DP samples, we refer to the original studies by](#) Lamping et al. (2021) and Vorrath et
182 al. (2020). The other part of the GDGT samples were analyzed on an Agilent 1260 Infinity II ultrahigh-performance liquid
183 chromatography-mass spectrometry (UHPLC-MS) system and a G6125C single quadrupole mass spectrometer. The
184 chromatographic separation was achieved by coupling two UPLC silica columns (Waters Acquity BEH HILIC, 2.1 × 150 mm,
185 1.7 µm) and a 2.1 × 5 mm pre-column as in Hopmans et al. (2016), but with the following chromatographic modifications:
186 Mobile phases A and B consisted of *n*-hexane: chloroform (99:1, v/v) and *n*-hexane: 2-propanol: chloroform (89:10:1, v/v/v),
187 respectively. The flow rate was set to 0.4 ml/min and the columns heated to 50° C, resulting in a maximum backpressure of
188 425 bar. Sample aliquots of 20 µl were injected with isocratic elution for 20 minutes using 86% A and 14% B, followed by a
189 gradient to 30% A and 70% B within the next 20 min. After this, the mobile phase was set to 100% B and the column rinsed
190 for 13 min, followed by 7 min re-equilibration time with 86% A and 14% B before the next sample analysis. The total run time
191 was 60 min.

192 IsoGDGTs were detected using positive ion APCI-MS and selective ion monitoring (SIM) of (M + H)⁺ ions (Schouten et
193 al., 2007) with the following settings: nebulizer pressure 50 psi, vaporizer and drying gas temperature 350° C, drying gas flow
194 5 L/min. The capillary voltage was 4 kV and the corona current +5 µA. The detector was set for the following SIM ions: *m/z*
195 744 (C₄₆ standard), *m/z* 1302.3 (GDGT-0), *m/z* 1300.3 (GDGT-1), *m/z* 1298.3 (GDGT-2), *m/z* 1296.3 (GDGT-3), *m/z* 1292.3
196 (Crenarchaeol and Cren' isomer). The resulting scan/dwell time was 66 ms.

197 4 Results and Discussion

198 [Our samples are located on a meridional transect along the Chilean margin extending into the DP, with changing environmental](#)
199 [conditions, in particular for SSTs, nutrients supply, salinity and current regimes. The U^K₃₇ values range from 0.07 \(PS97/079\)](#)
200 [to 0.38 \(PS97/132\), with minimum values in the southernmost region and increasing values to the north. All indices from](#)

hat nach oben verschoben [6]: As internal standard, 100 µl each of the *n*-alkane C₃₆ or 2-nonadecanone standard and C₄₆ were added before extraction.

hat gelöscht: 1%

hat gelöscht: extraction

hat gelöscht: of the samples of the Drake Passage

hat gelöscht: see

hat gelöscht: On our meridional transect along the Chilean margin, U^K₃₇ values

210 alkenones and *iso*GDTs are listed in [Table A2](#). In [Chapter 4.1 and 4.2](#), we compare the two most widely used calibrations
211 for alkenones in this region: the subpolar and polar SO Sikes97 calibration, as well as the Müller98 calibration [hereafter](#).

hat gelöscht: the following

hat formatiert: Schriftart: Fett, Englisch (USA)

212 4.1 Alkenone-based Sea Surface Temperatures

213 Alkenone-based SSTs calculated with Müller98 range from $\sim 10^\circ\text{C}$ in the northernmost locations of our study area to $\sim 1^\circ\text{C}$
214 in the southern part of the Drake Passage, south of the PF ([Figure 2A, B](#)). SST estimates based on Sikes97 instead range from
215 $\sim 12.5^\circ\text{C}$ in the northernmost locations to $\sim 4^\circ\text{C}$ in the Drake Passage ([Figure 2C, D](#)). Most values fit closely to the Müller98
216 calibration line of both, annual mean and summer SSTs, but show an offset to the Sikes97 calibration line ([Figure 3](#)). Although
217 Sikes97 was specifically adapted to the subpolar and polar SO, it generally overestimates modern SSTs in this study area, both
218 for annual mean and summer ([Figure 2](#) and [Figure 3](#)). Our samples for the SE Pacific fit well to Müller98, but not to Sikes97
219 ([Figure 2](#) and [Figure 3](#)). Because of the latter's overestimation of modern temperatures, we hereafter chose to solely use the
220 Müller98 calibration.

221 4.2 Influence of seasonality on alkenone temperature reconstruction

222 4.2.1 Seasonal signal along the Chilean Margin

223 Our alkenone-based SSTs fits world ocean atlas-derived annual mean and summer temperatures, showing only a small seasonal
224 effect towards warmer SSTs. This observation is also in line with previous data from the Northern – Central Chilean Margin,
225 which yields a slight seasonal effect south of 50°S (Prahl et al., 2006; Prahl et al., 2010). Also, a previous study from the
226 Chilean fjord region confirms SST signals being only slightly shifted towards summer in the southern Chilean fjord region
227 ([Figure 4](#); Caniupán et al., 2014). Along the Chilean continental margin, this seasonal summer effect even further decreases
228 southward to only $\sim 1^\circ\text{C}$ (i.e., summer SSTs vs. annual mean) between $50 - 57^\circ\text{S}$, based on WOA05-derived SSTs ([Figure](#)
229 [4](#); blue and yellow cross). This deviation of 1°C , at least north of the SAF, is within the generally accepted error range for
230 alkenone-derived paleo-SSTs of $\pm 1.5^\circ\text{C}$ (Müller et al., 1998), so that seasonality here appears to be negligible. Only further
231 south in the Drake Passage, deviations of our reconstructed summer temperatures from the annual mean increase to about 2°C ,
232 which are likewise reflected in WOA05-based SSTs ([Figure 4](#)). [Model results show a similar trend, with a small deviation](#)
233 [from the annual mean of up to \$2.5^\circ\text{C}\$ at higher latitudes as well](#) (Conte et al., 2006). [Such an increasing poleward seasonality](#)
234 [is not unusual due to a temporal shift of the alkenone production towards summer](#) (e.g., Volkman, 2000). [Another effect that](#)
235 [could be involved in the increased seasonality is the reduction in the diversity and quantity of coccolithophores through the](#)
236 [frontal system of the ACC](#) (e.g., Saavedra-Pellitero et al., 2014; Vollmar et al., 2022; Saavedra-Pellitero et al., 2019). [The](#)
237 [coccolithophore assemblages between the PF and the SAF show a significantly reduced diversity compared to north of the](#)
238 [SAF. South of the PF, coccolithophorids occur only sporadically and show a reduced diversity](#) (Saavedra-Pellitero et al., 2014).
239 [In this region, we are nearing the lower temperature end and thus ecological boundary conditions for coccolithophores. So,](#)

hat verschoben (Einfügung) [4]

hat gelöscht: The

hat gelöscht: of

hat gelöscht: in

hat gelöscht: on alkenone production is indicated by several studies based on coccolithophorids

246 alkenone production could be biased towards warmer years within the inevitably large time period of several hundreds of years
247 that is comprised in the uppermost centimeter of surface sediment.

248 In addition, not all data uniformly show a seasonal trend. The poleward increasing seasonal trend is discontinued by two
249 regions that reflect an annual mean instead (Figure 4; red circles). The first region is located between ~54 – 58° S near the
250 Strait of Magellan, where Atlantic waters mix with Pacific waters. The second region encompasses samples in the DP located
251 close to the PF. The PF marks the temperature boundary of the cold Antarctic surface water, which is subducted at the PF and
252 transported northwards (Orsi et al., 1995 - and references therein). This vertical water mass structure likely suppresses potential
253 seasonal effects by providing homogenous temperatures throughout the annual cycle, due to a reduce opportunity to build up
254 a warm summer surface layer.

255 This weakly expressed seasonality in our results, which remains mostly within the error range of Müller98, is in stark
256 contrast to results from other regions, notably the subarctic North Pacific. There, several studies showed a more consistent
257 seasonal shift towards summer and autumn SSTs of 4 – 6° C north of the subarctic front, while locations south of the subarctic
258 front reflect an annual mean (Max et al., 2020; Méheust et al., 2013; Prahl et al., 2010). The subarctic front in the North Pacific
259 acts as a natural boundary, creating a highly stratified subarctic surface ocean with a permanent halocline. In contrast, the
260 transition in the South Pacific from subtropical to polar regions is characterized by a lower salinity gradient and stratification,
261 leading to a less pronounced SAF. In the South Pacific instead, the year-round deep mixing within the ACC prevents the
262 formation of a prominent warm water layer during the summer. As a result, the former likely leads to pronounced seasonal
263 summer warming within strongly stratified surface waters, whereas the latter less stratified upper ocean would yield less
264 pronounced warming during austral summer months. Thus, subantarctic SSTs would be expected to show less seasonal
265 influence on their SST signal.

266 4.2.2 Regional **synthesis of** seasonality patterns across the South Pacific

267 We compared the samples from our relatively small study region with published data from the South Pacific Gyre, the Central
268 South Pacific, the New Zealand Margin (Jaeschke et al., 2017) and the Northern – Central Chilean Margin (Prahl et al., 2006;
269 Prahl et al., 2010) based on the Müller98 and Sikes97 calibrations (Figure 5). We also calculated the residual temperatures by
270 subtracting the modern WOA05 temperatures at 10 m water depth from our calculated temperatures, shown in combination
271 with $U^{K_{37}}$ against SSTs (Figure 5). The Central South Pacific and New Zealand Margin samples of Jaeschke et al. (2017)
272 spread over a wide area with different conditions. Taking into account a seasonal effect towards summer SSTs, only few
273 samples of this extended data set match with the Sikes97 calibration (Figure 5A, B; Jaeschke et al., 2017). This is partly in
274 contrast to Jaeschke et al. (2017) who concluded that alkenone-derived SSTs in general best reflect the austral summer months
275 when using Sikes97 calibration. The Müller98 calibration is applicable in the entire extended study area when compared with
276 both, annual mean and summer SSTs, reaffirming our decision to use Müller98 for further analyses.

277 The SCM and the Drake Passage samples are generally warmer by ~1.5° C than the samples from the Central South Pacific
278 region (Figure 6). The Central South Pacific samples represent a best fit to annual mean, in contrast to the SCM and DP

hat gelöscht: Our results reveal a rather localized structure that shows a general tendency towards a summer signal, except for two regions in our data set that reflect annual means instead

hat nach oben verschoben [4]: The effects of the frontal system in the ACC on alkenone production is indicated by several studies based on coccolithophorids (e.g., Saavedra-Pellitero et al., 2014; Vollmar et al., 2022; Saavedra-Pellitero et al., 2019). The coccolithophore assemblages between the PF and the SAF show a significantly reduced diversity compared to north of the SAF. South of the PF, coccolithophorids occur only sporadically and show a reduced diversity (Saavedra-Pellitero et al., 2014).

hat gelöscht: essentially

hat gelöscht: Furthermore

hat gelöscht: structure of the ACC and its

hat verschoben (Einfügung) [2]

hat gelöscht: Furthermore, the structure of the ACC and its year-round deep mixing prevents the formation of a prominent warm water layer during the summer.

hat nach oben verschoben [2]: Furthermore, the structure of the ACC and its year-round deep mixing prevents the formation of a prominent warm water layer during the summer.

hat gelöscht: In contrast, t

302 samples, which have a slight, but mostly negligible, seasonal shift toward summer SSTs (**Figure 6**). **The most likely reason**
 303 **for this bias** to summer SSTs in the SE-Pacific could be **a higher nutrient availability during the summer months due to the**
 304 **close proximity of the SE Pacific samples to South America. High nutrient availability could lead to a potentially changing**
 305 **competition between different primary producers, e.g., high silica input favors a diatom bloom, which changes when silica is**
 306 **depleted** (e.g., Durak et al., 2016; Smith et al., 2017; Tyrrell and Merico, 2004). **In this region, nutrient input is expected to be**
 307 **highest during austral summer months, when the high precipitation rates of 3,000 – 10,000 mm/yr in South Patagonia reach**
 308 **their maximum** (e.g., Garreaud et al., 2013; Lamy et al., 2010; Schneider et al., 2003). The increased precipitation during
 309 **summer months results in an increased freshwater runoff** (e.g., Dávila et al., 2002), accompanied by increased supply of
 310 **continent-derived nutrients to hemipelagic and DP waters and a more stable seasonal thermocline** (Toyos et al., 2022), **which**
 311 **would both** favor a seasonal coccolithophore bloom.

312 The area off New Zealand correlates well with samples off the Northern – Central Chilean Margin north of ~45° S and
 313 corresponds to the annual mean (**Figure 6**). In contrast, the South Pacific Gyre samples reflect a summer to autumn signal
 314 (**Figure 6**; Jaeschke et al., 2017). **The South Pacific Gyre is characterized by** extremely low nutrient content and accordingly
 315 low primary production (D'hondt et al., 2009). **Reasons for the low nutrient content here are the distance** from potential
 316 continental inputs, **and a relatively deep thermocline setting, which reduces upwelling and nutrient advection** (D'hondt et al.,
 317 2009; Lamy et al., 2014). **This is reflected by** low alkenones, *n*-alkanes and **branched (br)GDGTs** concentrations (Jaeschke et
 318 al., 2017). These factors likely lead to a seasonal bias if e.g., dust transport and macronutrient supply are increased in late
 319 spring to summer, **and** relatively quickly exhausted.

320 4.3 GDGT – based (sub)surface temperatures

321 Similar to U^{K-37} values, **isoGDGT**-derived indices $TEX^{H_{86}}$ and $TEX^{L_{86}}$ increase along our transect from south to north. The
 322 values range from -0.48 to -0.61 (PS97/079) and from -0.39 to -0.53 (PS97/131) for $TEX^{H_{86}}$ and $TEX^{L_{86}}$, respectively (cf.
 323 **Table A2**). In contrast to Coccolithophorids, *Thaumarchaeota* live at greater water depths (e.g., Karner et al., 2001) and occur
 324 **also in the polar regions** (e.g., Massana et al., 1998; Murray et al., 1998), which complicates the choice of an adequate
 325 temperature calibration, since reference data and sample sites for both characteristics remain scarce. For the **isoGDGTs**, we
 326 use six calibrations in total for both indices: the surface calibrations $SST^{H_{Kim}}$, $SST^{H_{Kaiser}}$ and $SST^{L_{Kim}}$, as well as the
 327 subsurface calibrations $Tsub^{H_{Kim}}$, $Tsub^{H_{Kaiser}}$ and $Tsub^{L_{Kim}}$ (**Table A1**).

328 Surface and subsurface ranges for **isoGDGTs** are following the definition of Kaiser et al. (2015), Kim et al. (2012b) and
 329 Kim et al. (2012a), with a mean of 0 – 50 m water depth and 0 – 200 m water depth, respectively. We therefore used the
 330 WOA05-derived temperatures of depths from 10 m and 125 m for surface and subsurface, as they roughly correspond to the
 331 average values (**Figure 7**). Based on the surface calibrations, the temperatures range from ~11.5° C to 5° C for $SST^{H_{Kim}}$,
 332 from ~9.5° C to 4° C for $SST^{H_{Kaiser}}$, and from ~13° C to 6° C for $SST^{L_{Kim}}$. With the subsurface calibrations, the
 333 temperatures range from ~9° C to 4° C for $Tsub^{H_{Kim}}$, ~9° C to 5° C for $Tsub^{H_{Kaiser}}$, and from ~10° C to 5° C for $Tsub^{L_{Kim}}$
 334 (**Figure 7**).

hat gelöscht: tendency

hat gelöscht: due to several factors like changes in the current and wind regimes, or nutrient availability, leading to a potentially changing competition between different primary producers. Such

hat gelöscht: might be amplified by the close proximity of the SE Pacific samples to South America

hat gelöscht: where

hat gelöscht: in South Patagonia during the summer months

hat gelöscht: the

hat gelöscht: Drake passage

hat gelöscht: . In addition, higher stratification by an increased freshwater supply due to the proximity to the continental shelf

hat gelöscht: These latter sample locations are characterized by an

hat gelöscht: Due to the

hat gelöscht: pelagic setting

hat gelöscht: other than through dust,

hat gelöscht: with

hat gelöscht: only

hat gelöscht: little

hat gelöscht: and upwelling occurs in this area

hat gelöscht: as evidenced

hat gelöscht: , but

hat gelöscht: before a sustained alkenone production would record an annual mean temperature signal, due to the deep and stable thermocline inhibiting further macronutrient supply

hat formatiert: Schriftart: Fett

hat formatiert: Schriftart: Fett

hat gelöscht: at higher latitudes

hat formatiert: Schriftart: Fett, Englisch (USA)

hat formatiert: Englisch (USA)

hat formatiert: Schriftart: Fett, Englisch (USA)

361 The locations north of the SAF fit best to the modern WOA05-derived SSTs with the SST^HKaiser calibration (**Figure 7B**)
362 and appear to extend the surface regression line along the 5 – 10° C temperature range (**Figure 8A**). On average, the modern
363 temperatures are overestimated by ~1.3° C, which means they are no longer within the ±0.8° C standard error determined by
364 Kaiser et al. (2015) for the surface calibration. In the subsurface, the Tsub^HKim and Tsub^HKaiser calibrations equally fit the
365 modern WOA05-derived Tsub (**Figure 7D, E**), but the samples tend to fit better with the calibration line of Tsub^HKim (**Figure**
366 **8B**). On average, the modern WOA05-derived Tsub are overestimated here by ~1.6° C. Thus, the calculated temperatures are
367 within the of ±2.2° C error range given by Kim et al. (2012a), but not within the ±0.6° C given by Kaiser et al. (2015) for the
368 subsurface calibration. The samples from the DP instead do not fit to any calibration and overestimate modern WOA05-derived
369 SSTs or Tsub in all calibrations, [leading us to compare our results to other previously published data \(see Chapter 4.5: Figure](#)
370 [7 and Figure 8](#)).

371 Apart from absolute temperature values, the slope of various calibrations ~~allows to~~ calculate relative temperature changes
372 ~~through time in marine sediment cores. Hence, the slope of the used temperature calibration in an area should adequately~~
373 ~~resemble the magnitude of relative temperature changes (e.g., between glacial and interglacial periods) to provide correct ΔT,~~
374 ~~which is e.g., often used in modelling studies (Burke et al., 2018), even if absolute temperature are offset.~~ To determine which
375 calibration best captures relative temperature changes in our study region, we compared our samples with published data from
376 the Central South Pacific and New Zealand Margin (Ho et al., 2014; Jaeschke et al., 2017), in addition to the Northern – Central
377 Chilean Margin (Kaiser et al., 2015) dataset (**Figure 9**). In **Figure 9A – D** we show in red the regressions of all sites located
378 north of the SAF (called “local regression” hereafter) in comparison to the published six different SST and Tsub calibrations
379 of both Kim et al. (2010, 2012a and b), and Kaiser et al. (2015). In addition, we show the residuals in **Figure 9E, F** to illustrate
380 which data are within the error range of the respective calibrations. For this purpose, the mean WOA05 values of 0 – 50 m and
381 0 – 200 m of the annual mean were subtracted from the respective temperature calibration.

382 The slope of the SST^HKim calibration shows a difference of ~3.2 to our local regression (**Figure 9A**), and yields best the
383 relative temperature change across the region north of the SAF, although it generally yields the highest residuals (**Figure 9E**).
384 The Tsub^HKim calibration, with a difference of ~3.9 between the two slopes (**Figure 9C**), captures the relative temperature
385 changes as well. The latter corresponds to a temperature change (TEX^H₈₆: -0.2 to -0.3) of 5.5° C with Tsub^HKim and 5.1° C
386 with our local regression. In contrast to SST^HKim, the residuals are smaller and within the reported error range of ±2.2° C
387 (Kim et al., 2012a) for most samples north of the SAF (**Figure 9F**). Again, the central South Pacific samples located south of
388 the SAF significantly overestimate local SSTs or Tsub with annual residuals of ~8.4° C (SST^HKim), ~6.6° C (SST^HKaiser),
389 ~8.1° C (SST^LKim), ~6.4° C (Tsub^HKim), ~6.9° C (Tsub^HKaiser) and ~6.7° C (Tsub^LKim).

390 Thus, our combined sample set north of the SAF fits the Tsub^HKim calibration best, while the samples south of the SAF
391 do not match the commonly used calibrations, including the two calibrations based on TEX^L₈₆ for (sub)polar regions (Kim et
392 al., 2012b; Kim et al., 2010).

- hat gelöscht: which often yield offsets to instrumental data (REF).
- hat gelöscht: provides
- hat gelöscht: the potential to
- hat gelöscht: in time series
- hat gelöscht: Meaning that as long as
- hat gelöscht: required
- hat gelöscht: is similar to the usual calibrations,
- hat gelöscht: regardless of their position in the coordinate system,
- hat gelöscht:) will still be
- hat gelöscht: would
- hat gelöscht: be
- hat gelöscht: off

405 **4.4 Influence of habitat depth and terrestrial input on *Thaumarchaeota*-derived temperatures**

406 Habitat depth preferences for *Thaumarchaeota* and their response to seasonality (e.g., Schouten et al., 2013a) may influence
407 the TEX₈₆-derived temperature signals. Since *Thaumarchaeota* are distributed throughout the entire water column, the
408 decision to choose an optimal calibration is closely linked to an initial assumption about the water depth from which the signal
409 originates (Kamer et al., 2001). Hence, we applied the ratio of GDGT-2 to GDGT-3 (GDGT [2]/[3]) to locate the water depth
410 of the temperature signal, since subsurface dwelling *Thaumarchaeota* preferentially yield GDGT-2 over the GDGT-3 (Kim et
411 al., 2015; Taylor et al., 2013).

412 In the global ocean the distribution of *Thaumarchaeota* appears to vary within the water column and shows an increasing
413 GDGT [2]/[3]-ratio with increasing depth (Dong et al., 2019; Hernández-Sánchez et al., 2014; Kim et al., 2015; Kim et al.,
414 2016; Schouten et al., 2012; Taylor et al., 2013). Water column samples in the Arabian Sea and along the Portuguese margin
415 show a GDGT [2]/[3]-ratio between <3.3 in the upper 50 m and 4.0 – 21.5 at >200 m water depth (Dong et al., 2019; Kim et
416 al., 2016; Schouten et al., 2012). In the South China Sea, the GDGT [2]/[3]-ratio yields <3.5 at <100 m water depth and
417 5.9 – 8.6 at water depth >300 m (Dong et al., 2019). In the Southeast Atlantic, the GDGT [2]/[3]-ratio of between 0 – 50 m
418 water depth is 1.9 – 3.4, 4.1 – 12.8 between 50 – 200 m water depth and 13 – 50 in water depth >200 m (Hernández-Sánchez
419 et al., 2014). Thus, increasing GDGT [2]/[3]-ratios may not be strictly coupled to water depths across the world ocean. The
420 GDGT [2]/[3]-ratio in the surface area seems similar in all regions with ~3.5, but subsurface values differ considerably. In the
421 Southern Atlantic, the GDGT [2]/[3]-ratio increases to up to 12.8 within 50 – 200 m water depth, whereas at the Portuguese
422 margin, the Arabian and the South China Sea, the GDGT [2]/[3]-ratio increases up to ~5.0, with oxygen content or nutrients
423 being the most likely reason for such non-linearities (e.g., Basse et al., 2014; Villanueva et al., 2015).

424 The GDGT [2]/[3]-ratios in our extended study area vary between ~3 – 25. Values <5 (n = 7), indicating a surface signal,
425 are found only occasionally off New Zealand and along the Chilean Margin. The majority of samples would correspond to a
426 subsurface signal with a GDGT [2]/[3]-ratio >5, confirming our calibration choice (Tsub^HKim) for the South Pacific. Studies
427 from the Humboldt Current system, the Antarctic Peninsula and the North Pacific Gyre confirm this assumption and indicate
428 a subsurface rather than a surface signal (Kalanetra et al., 2009; Karner et al., 2001; Massana et al., 1998; Quiñones et al.,
429 2009). Here, we will distinguish between shallower subsurface (0 – 200 m water depth) and deep subsurface (>200 m water
430 depth), to quantify the influence of deep subsurface-dwelling *Thaumarchaeota* to the GDGT distribution in the sediment. In
431 general, it is assumed that a deep subsurface water influence is comparatively small, since *Thaumarchaeota* can be most
432 effectively grazed, packed into fecal pellets, and transported to the seafloor within the photic zone (Wuchter et al., 2005).
433 Nevertheless, variations in the GDGT [2]/[3]-ratio across the entire study area can provide information about regions that may
434 be subject to a greater influence of deep subsurface dwelling *Thaumarchaeota*. Our South Pacific locations yield differences
435 in GDGT [2]/[3]-ratio according to three principally differing boundary or forcing conditions: A hemipelagic continental
436 margin setting, a deep thermocline oligotrophic gyre setting, and a SO frontal setting (Figure 10).

hat gelöscht: In the following

438 In the overall study area, our results suggest that isoGDGTs record shallower subsurface temperatures rather than surface
 439 temperatures. Samples along continental slopes tend to be less influenced by deep subsurface-dwelling *Thaumarchaeota*, while
 440 samples from the pelagic regions show a greater influence by deep subsurface-dwelling *Thaumarchaeota*. Samples along the
 441 Chilean Margin yield a mean GDGT [2]/[3]-ratio of ~6.2 to ~6.9, reflecting a transition between surface and shallow subsurface
 442 habitats. This is in line with Northern – Central Chilean Margin data, which show a positive correlation with both SSTs and
 443 Tsub (Kaiser et al., 2015). The amount of deep subsurface-dwelling *Thaumarchaeota* increase with increasing distance from
 444 land, as shown by samples from the SW Pacific close to New Zealand. The GDGT [2]/[3]-ratios increase, in line with Taylor
 445 et al. (2013), from ~3.1 at ~600 m water depth to ~9.8 at >3000 m water depth to ~12.9 at >4000 m water depth (Figure 10).
 446 The highest influence of deep-dwelling *Thaumarchaeota* occurs in the South Pacific Gyre and in the eastern South Pacific,
 447 averaging a GDGT [2]/[3]-ratio of ~11.5 and indicating a potentially larger contribution of deep subsurface-dwelling
 448 *Thaumarchaeota* communities in the sediment, but no significant temperature deviations can be detected for the region north
 449 of the SAF (Figure 9). This suggests either that the influence of the deep subsurface-dwelling *Thaumarchaeota* on the
 450 temperature signal is smaller than previously thought, or that the distribution of the GDGT [2]/[3]-ratio in the subsurface in
 451 this region differs from that in the central South Pacific or continental margins.

452 Besides contributions from deeper living *Thaumarchaeota*, the GDGT [2]/[3]-ratio can also be influenced by isoGDGTs
 453 derived from terrestrial soils and peats, where the amount of the GDGT-3 is increased compared to the marine milieu (Weijers
 454 et al., 2006). This would result in GDGT [2]/[3]-ratio decreases with increasing terrestrial input, i.e., in the opposite direction
 455 of the influence of deeper living *Thaumarchaeota*. Therefore, we compared the GDGT [2]/[3]-ratios with monthly average
 456 dust depositions (Figure 12) and found high GDGT [2]/[3]-ratios in areas with very little dust accumulation and lower GDGT
 457 [2]/[3]-ratios with higher dust accumulation. This could explain the discrepancy between eastern and western pelagic South
 458 Pacific at a first glance and fit also to the low GDGT [2]/[3]-ratios along continental margins. To detect such distortions of
 459 terrigenous isoGDGTs on the GDGT [2]/[3]-ratio and therefore the TEX-based indices, the branched vs isoprenoid tetraether
 460 (BIT; should be <0.3) index was developed, where the brGDGTs occurring predominantly in terrestrial soils are related to the
 461 Crenarchaeol (Hopmans et al., 2004). The BIT is low (<0.1) in this region, indicating no significant influence from land
 462 (Jaeschke et al., 2017; Kaiser et al., 2015). The nearly perfect fit of the GDGT [2]/[3]-ratios with dust distribution indicates
 463 that future studies should more systematically address underlying causes of these co-variations, at least in regions with low
 464 sedimentation rates but high potential eolian transport. Generally however, isoGDGT-derived temperatures of samples north
 465 of the SAF fit quite well with Tsub^{Kim}, so that both potential influences, deeper-dwelling *Thaumarchaeota* as well as
 466 terrigenous input seems to be negligible.

4.5 Towards an alternative southern hemisphere (sub)-polar calibration for isoGDGT-based temperatures

468 IsoGDGTs south of the SAF appear to have a lower sensitivity to temperature, which is in line with previous results,
 469 showing a large scatter of the TEX₈₆ – SST relationship in the polar regions (e.g., Kim et al., 2010; Fietz et al., 2020 and
 470 references therein). One reason given for the larger scatter may be a calibration based on satellite-assigned SSTs, which in

hat verschoben (Einfügung) [5]

hat gelöscht: The highest influence of deep-dwelling *Thaumarchaeota* occurs in the South Pacific Gyre. In the SE Pacific

hat gelöscht: the GDGT [2]/[3]-ratio increases with increasing latitudes. Samples along the Chilean Margin (Kaiser et al., 2015)

hat gelöscht: which implies a shallow subsurface (≥50 m water depth) habitat, with a potential increase in the amount of deeper-dwelling *Thaumarchaeota* from north to south, in line with previous studies (Quiñones et al., 2009). On the other hand, t

hat gelöscht: , and the surface calibration has a comparable slope with suspended particulate matter close to the surface

hat gelöscht: We assume that along the Chilean Margin and SCM, the TEX₈₆ and TEX₈₆ signal reflects a transition between surface and shallow subsurface habitats, where shallow subsurface habitats increasingly prevail towards higher latitudes. Additionally, t

hat gelöscht: e.g., site PS97/114 on the SCM is located further offshore and yields a GDGT [2]/[3]-ratio of 10.6 (3863 m water depth) compared to the mean of ~6.9 at ~1700 m water depth closer to the margin. Our assumption is supported by our own results from the

hat gelöscht: , which are a good example for

hat gelöscht: increasing sedimentary

hat gelöscht: with increasing water depths

hat gelöscht: , in line with a study by Taylor et al. (2013). The SW Pacific samples close to the margin show a GDGT [2]/[3]-ratio of ~3.1 (~600 m water depth), indicating surface temperature signals. With greater distance from the margin, the GDGT [2]/[3]-ratio increases to ~9.8 (>3000 m water depth) or ~12.9 (>4000 m water depth), and thus the influence of deep subsurface-dwelling *Thaumarchaeota*.

hat gelöscht: On the other hand,

hat gelöscht: In the Drake Passage, the GDGT [2]/[3]-ratios show average values of ~8.7 and are mostly higher than on the Chilean Margin, implying a more prominent influence of deep subsurface-dwelling *Thaumarchaeota* (Figure 10). We found GDGT [2]/[3] maxima close to the PF (~10.1), probably caused by stronger mixing, which would result in a higher abundance of deep subsurface-dwelling *Thaumarchaeota* below the northward-flowing Antarctic Surface Water layer. Values around the SACCF are ~6.7, comparable to those on the SCM, and therefore likely represent shallow subsurface habitats, with only minor influence from deep subsurface-dwelling *Thaumarchaeota*. This is in line with evidence from the Antarctic Peninsula region, which shows highest abundances of *Thaumarchaeota* between ca. 40 – 100 m water depth in Antarctic Winter Water and a near-absence in the surface layer (Kalanetra et al., 2009). Samples from the Southwest Pacific (Ho et al., 2014; Jaeschke et al., 2017) show comparable results, with slightly lower mean GDGT [2]/[3]-ratios of ~8 and absolute minima of ~6.4 south of the SACCF (Figure 10).

hat gelöscht: In summary,

hat nach oben verschoben [5]: our results suggest that GDGTs record shallower subsurface temperatures rather than surface temperatures in the study area. Samples along continental slopes tend to be less influenced by deep subsurface-dwelling *Thaumarchaeota*,

532 polar regions yields values below the freezing point of seawater (Pearson and Ingalls, 2013). Consequently, a larger scatter of
533 polar samples leads to a larger error of estimate in the related calibrations and would explain the occurrence of highest residuals
534 with SST^HKim and SST^LKim in our study area in both north and south of the SAF (Figure 7, 9), i.e., where calibrations are
535 based on satellite-assigned SSTs. However, our data does not show an increased scatter of values south of the SAF. Instead,
536 they show a different TEX^H₈₆ (TEX^L₈₆) – water temperature relationship, resulting in a lower slope of the calibration line
537 (Figure 9).

538 We suspect that the SAF acts as a natural boundary, leading to differential responses within the *Thaumarchaeota*
539 communities and their respective isoGDGTs to changing environmental parameters such as pH (Elling et al., 2015) or oxygen
540 availability (Qin et al., 2015). Another reason for this pattern could be the increased occurrence of OH-isoGDGTs in polar
541 regions. OH-isoGDGTs are present in lower amounts in the sediment than the isoGDGTs used in TEX^H₈₆ and TEX^L₈₆, but are
542 most abundant in higher latitudes (Fietz et al., 2013; Huguet et al., 2013; Liu et al., 2020). This increased occurrence of OH-
543 isoGDGTs could indicate an adaptation to cold temperatures to maintain membrane fluidity. This could simultaneously affect
544 the relationship of TEX-based indices to temperature, requiring a separate calibration for high latitudes. OH-isoGDGTs also
545 show a stronger correlation with water temperature than isoGDGTs in both the Arctic (Fietz et al., 2013) and close to Antarctica
546 (Liu et al., 2020), so another OH-isoGDGT-based index RI-OH' (= [OH-GDGT-1]+2*[OH-GDGT-2]/[OH-GDGT-0]+[OH-
547 GDGT-1]+[OH-GDGT-2]; SST = (RI-OH' - 0.1)/0.0382) has been proposed for polar regions (Lü et al., 2015). Moreover, OH-
548 isoGDGTs were often not measured in legacy samples reported in early studies. Based on this, Fietz et al. (2020) recommended
549 a multi-proxy approach for the polar regions, which includes both isoGDGTs and OH-isoGDGTs. However, isoGDGTs were
550 more commonly used and OH-isoGDGTs may not be available for some data sets. A good example are the data sets (e.g.)
551 Tsub^LKim with n = 396 (Kim et al., 2012b) and RI-OH'-based surface calibration with n = 107 (Lü et al., 2015), which are
552 designated for the same temperature range <15° C. A working TEX-based calibration specifically developed for the SO is
553 therefore appropriate and may also be useful for further research on the functionality (OH)-isoGDGTs. Therefore, we here
554 take an initial step and propose a modified TEX-based cold temperature calibration for the southern hemisphere (sub)polar
555 region. We will then test the new calibration by (1) re-estimating the temperatures of a published sediment core and (2)
556 comparing the SSTs and Tsub determined with the new calibration to RI-OH'-based SSTs.

557 This suggested calibration includes samples south of the SAF in the SO, and is extended by the data sets of Kim et al.
558 (2010) and Lamping et al. (2021) with a total of n = 137 samples. Changes in TEX^H₈₆ or general TEX₈₆ indices below 5° C
559 water temperature (according to SSTs south of the SAF in the Southern Ocean) are less pronounced than above 5° C, because
560 of a weaker correlation of the isomer Cren' to water temperatures. Thus, it is excluded in the TEX^L₈₆ – index as proposed by
561 earlier studies (Kim et al., 2010). This is in line with our results, where all TEX^L₈₆ calibrations show a stronger correlation
562 than those based on TEX^H₈₆ (cf. determination coefficient R²; Figure 11). The maximum R² value of 0.7 (TEX^L₈₆, subsurface)
563 is only slightly lower than previously published values (>0.8, cf.; Table A1), which is to be somewhat expected, because the
564 scatter of both TEX^H₈₆ and TEX^L₈₆ indices below 5° C seems to be generally larger (Ho et al., 2014).

hat gelöscht: so

hat gelöscht: might better represent relative temperature changes

hat gelöscht: . The

hat formatiert: Schriftart: Fett

hat formatiert: Schriftart: Fett

568 Based on our results, we propose a new TEX^{L}_{86} – based annual mean, subsurface (0 – 200 m) and surface (0 – 50 m)
569 calibration for the Southern Ocean’s polar and subpolar regions:

570
571 $T_{sub} = 14.38 * TEX^{L}_{86} + 8.93,$ (1)

572 $SST = 10.71 * TEX^{L}_{86} + 6.64,$ (2)

573
574 The standard error of $\pm 0.6^{\circ} C$ ($\pm 0.5^{\circ} C$) for our subsurface (surface) calibration is lower than the standard error from the
575 previous subsurface (surface) calibration $T_{sub}^{L}Kim$ ($SST^{L}Kim$) with $\pm 2.8^{\circ} C$ ($\pm 4^{\circ} C$), which is probably due to the latter’s
576 lower data density. With this new calibration, just 44 (40) of the 137 samples lie outside this error range. Another major
577 difference between our calibration and $T_{sub}^{L}Kim$ ($SST^{L}Kim$) is the slope of the regression line being much flatter here at 14.4
578 (10.7) than the slope of the calibration $T_{sub}^{L}Kim$ ($SST^{L}Kim$) with 50.8 (67.5) (**Figure 9**). This leads to a generally smaller
579 temperature increase with an increasing TEX^{L}_{86} index. An increase of TEX^{L}_{86} from -0.6 to -0.5 e.g., corresponds to a
580 temperature change of $1.4^{\circ} C$ in our subsurface calibration and of $5.1^{\circ} C$ in $T_{sub}^{L}Kim$.

581 (1) Using our new calibration, we compare recalculated results with the previously used subsurface TEX^{L}_{86} calibration
582 $T_{sub}^{L}Kim$ (**Figure 13**) on core MD03-2601 ($66^{\circ}03.07' S$, $138^{\circ}33.43' E$; Kim et al., 2012b) from the eastern Indian sector of
583 the SO covering the Holocene, where the authors acknowledged that a temperature offset existed, but within the specified
584 calibration error range of $\pm 2.8^{\circ} C$. Temperatures based on our subsurface calibration are on average $\sim 2.5^{\circ} C$ colder than the
585 ones based on the previously used subsurface calibration $T_{sub}^{L}Kim$. With our new calibration, temperatures remain relatively
586 constant at $-0.8^{\circ} C$, and at $1.5^{\circ} C$ with the subsurface calibration $T_{sub}^{L}Kim$ between 4.8 – 3.1 ka BP. Modern temperatures
587 near the core site agree well with core top results from our new calibration with $-0.7^{\circ} C$ ($65.5^{\circ} S$, $138.5^{\circ} E$; Locarnini et al.,
588 2006) vs. $-0.8^{\circ} C$ (our reconstruction) for the subsurface layer. The recalculated temperature increases, associated with warmer
589 nutrient-rich modified Circumpolar Deep-Water intrusions, show an attenuated amplitude with the new calibration
590 (**Figure 13**). The amplitude based on our new calibration is $1.2^{\circ} C$ around 1.7 ka BP, whereas it is $4.2^{\circ} C$ with the original
591 subsurface calibration $T_{sub}^{L}Kim$ and therefore better fits to the expected temperatures.

592 (2) While we do not have OH-isoGDGTs for the Kim et al. (2010), Jaeschke et al. (2017) and Ho et al. (2012) datasets, we
593 calculated SSTs based on the RI-OH’ index and compared them to SSTs and T_{sub} based on our calibrations for all samples
594 south of the SAF for which OH-isoGDGTs are available (Drake Passage, Antarctic Peninsula, Wedell Sea and Amundsen
595 Sea). The results of all three calibrations (TEX^{L}_{86} -based SST and T_{sub} ; RI-OH’-based SST) fit (**Figure 14**), with a temperature
596 discrepancy of $\pm 1^{\circ} C$ from each other. One exception here is the Drake Passage, where the RI-OH’-based SSTs show residuals
597 of $> 2^{\circ} C$. Considering the standard error of $\pm 6^{\circ} C$ (Lü et al., 2015), all RI-OH’-based SSTs are within this error range. The
598 upper ocean temperatures in the Drake Passage are the only ones in this area above zero, which may explain the larger residuals
599 of the RI-OH’-based SSTs. It is possible that similar to the subsurface calibration of Kim et al. (2012b), the relative temperature
600 change is not correctly captured due to a too steep regression line for samples south of the SAF. The calibration of Lü et al.

hat verschoben (Einfügung) [3]

hat gelöscht: Kim et al. (2010), Ho et al. (2012), and Jaeschke et al. (2017)

hat gelöscht: , which also include samples south of the SAF. Furthermore

hat gelöscht: we calculated SSTs based on the RI-OH’ index and compared them to SSTs and T_{sub} based on our calibrations

hat nach oben verschoben [3]: We do not have OH-isoGDGTs for the Kim et al. (2010), Ho et al. (2012), and Jaeschke et al. (2017) datasets, which also include samples south of the SAF.

hat gelöscht: well together

hat gelöscht: water

hat gelöscht: dataset

hat gelöscht: that are

614 (2015) includes only a few samples from higher latitudes, most of them from the Arctic, and samples in the temperature range
615 between 1 – 3° C are almost absent. A RI-OH'-based calibration for samples south of the SAF could increase the sensitivity
616 of the proxy and decrease the standard error, similar to the TEX^L₈₆-index demonstrated here. This is in contrast to the good
617 agreement of the remaining samples, both with our TEX-based temperature reconstructions and with the WOA05-derived
618 temperatures. A calibration based on TEX^L₈₆ developed specifically for the SO yields comparable results to a calibration based
619 on OH-isoGDGTs. We agree with Fietz et al. (2020) to determine both indices, if possible, as this is a good way to check the
620 consistency of temperature reconstructions.

622 5 Conclusion

623 In this study, we provide a qualitative evaluation of the most common temperature calibrations for alkenones and
624 isoGDGTs in the South Pacific and potential environmental influencing factors. For alkenone-derived SSTs, our results
625 provide a best fit with the global core-top calibration of Müller et al. (1998). On a regional scale, the Southern Chilean Margin
626 and the Drake Passage show a small seasonal effect of ~1° C towards warmer SSTs south of ~50° S, albeit well within the
627 ±1.5° C standard error for alkenone derived SSTs (Müller et al., 1998). Excluding local influences, the seasonal effect in the
628 DP is slightly higher at about ~2° C and no longer within the error range of calibration by Müller et al. (1998). In contrast, the
629 samples from the Central Southern Pacific Ocean show no clear seasonal trend. Causes for this difference between the two
630 areas are increased seasonal provision of nutrients, or more pronounced stratification at the sites proximal to continental runoff
631 along the Chilean margin during late summer time.

632 IsoGDGT-based temperatures show a more complex pattern, which necessitates choosing the temperature calibration
633 carefully, depending on the area. The optimal calibration for isoGDGT-based temperature reconstructions in the South Pacific
634 is the subsurface calibration Tsub (Kim et al., 2012a), for samples north of the Sub-Antarctic Front, in line with evidence from
635 compiled GDGT [2]/[3]-ratios, which indicate a subsurface of 0 to 200 m water depth, rather than surface habitat depth
636 throughout the study area. South of the Sub-Antarctic Front, all existing calibrations overestimate local WOA05-derived
637 temperatures. Furthermore, the GDGT [2]/[3]-ratios do also correlate with the average monthly dust deposition in the South
638 Pacific. A new calibration for subpolar and polar areas yields lower absolute subsurface temperatures, as well as lower relative
639 changes within the commonly accepted standard error range. The results of this new calibration fit well within the standard
640 error with OH-GDGT-derived temperatures.

641 For future work, we recommend to extend both the geographical area coverage in subpolar and polar regions and the sample
642 density. Furthermore, the influence of seasonality and habitat should be investigated to assess how strongly these factors affect
643 paleo-temperature reconstructions.

hat gelöscht: In this study, we provide a new surface sediment dataset of alkenone- and GDGT-derived temperatures from the Southern Chilean Margin and the Drake Passage. In combination with previously published results from the Southern Ocean, we expanded our study area and examined which underlying calibration solution to determine upper ocean temperatures works best. In addition, we studied the possible influence of seasonal effects and the habitat water depth on the derived temperature reconstructions. ¶ For alkenone-derived SSTs, our

hat gelöscht: ¶ As a result, we recommend to establish two new Southern Ocean calibrations for GDGT-based temperature reconstructions and attempt to improve temperature calculations for the Pacific sector of the Southern Ocean, based on the TEX^L₈₆ index. Our

hat gelöscht: when compared to instrumental reference data

hat gelöscht: Since our study was restricted to a mostly regional dataset

hat gelöscht: for future works

hat gelöscht: on signal incorporation

hat gelöscht: based on GDGTs

664 Appendix A

665 Table A1: Common indices and their most important temperature calibrations for alkenones and isoGDGTs, with their
 666 determination coefficients (R^2) and abbreviations used in this paper. $U^{K'_{37}}$ = Alkenone unsaturation index consisting of 37 carbon
 667 atoms; TEX_{86} = Tetraether index consisting of 86 carbon atoms; TEX_{86}^H = Tetraether index for water temperatures above 15° C;
 668 TEX_{86}^L = Tetraether index for water temperatures below 15° C; SST = Sea Surface Temperature; Tsub = Sea subsurface
 669 temperatures (0 – 200 m water depth). Abbreviation: the here defined abbreviations will be used in the main text.

	Equation	R^2	Abbreviation	References
1	$U^{K'_{37}} = [C_{37:2}] / [C_{37:2}] + [C_{37:3}]$			Prahl and Wakeham (1987)
2	$SST = (U^{K'_{37}} - 0.043) / 0.033$	0.994		Prahl and Wakeham (1987)
3	$SST = (U^{K'_{37}} - 0.039) / 0.034$	0.994	Prahl88	Prahl et al. (1988)
4	$SST = (U^{K'_{37}} - 0.044) / 0.033$	0.958	Müller98	Müller et al. (1998)
5	$SST = (U^{K'_{37}} + 0.082) / 0.038$	0.921	Sikes97	Sikes et al. (1997)
6	$TEX_{86} = \frac{[2] + [3] + [Cren']}{[1] + [2] + [3] + [Cren']}$			Schouten et al. (2002)
7	$TEX_{86}^H = \log \frac{[2] + [3] + [Cren']}{[1] + [2] + [3] + [Cren']}$			Kim et al. (2010)
8	$TEX_{86}^L = \log \frac{[2]}{[1] + [2] + [3]}$			Kim et al. (2010)
9	$SST = 68.4 * TEX_{86}^H + 38.6$	0.87	SST ^H Kim	Kim et al. (2010)
10	$Tsub = 54.7 * TEX_{86}^H + 30.7$	0.84	Tsub ^H Kim	Kim et al. (2012a)
11	$SST = 59.6 * TEX_{86}^H + 33$	0.91	SST ^H Kaiser	Kaiser et al. (2015)
12	$Tsub = 32.1 * TEX_{86}^H + 21.5$	0.86	Tsub ^H Kaiser	Kaiser et al. (2015)
13	$SST = 67.5 * TEX_{86}^L + 46.9$	0.86	SST ^L Kim	Kim et al. (2010)
14	$Tsub = 50.8 * TEX_{86}^L + 36.1$	0.87	Tsub ^L Kim	Kim et al. (2012b)

670

671 **Table A2: Surface sediment sample results of this study.** $U^{K'_{37}}$ = Alkenone unsaturation index consisting of 37 carbon atoms; TEX_{86}
672 = Tetraether index consisting of 86 carbon atoms; TEX_{86}^H = Tetraether index for water temperatures above 15° C; TEX_{86}^L =
673 Tetraether index for water temperatures below 15° C.

	Station	Latitude	Longitude	Depth [m]	$U^{K'_{37}}$	TEX_{86}^H	TEX_{86}^L
<i>Southern Chilean Margin</i>							
1	PS97/139-1	52° 26.56' S	75° 42.42' W	640	0.40	-0.40	-0.58
2	PS97/134-1	52° 40.97' S	75° 34.85' W	1075.1	0.36	-0.39	-0.54
3	PS97/132-2	52° 37.01' S	75° 35.14' W	843	0.38	-0.47	-0.60
4	PS97/131-1	52° 39.58' S	75° 33.97' W	1028.2	0.35	-0.39	-0.53
5	PS97/129-2	53° 19.28' S	75° 12.84' W	1879.4	0.34	-0.41	-0.54
6	PS97/128-1	53° 38.04' S	75° 32.71' W	2293.7	0.32	-0.42	-0.54
7	PS97/122-2	54° 5.85' S	74° 54.89' W	2560	0.31	-0.41	-0.53
8	PS97/114-1	54° 34.68' S	76° 38.85' W	3863	0.26	-0.41	-0.50
9	PS97/027-1	54° 23.05' S	74° 36.30' W	2349.2	0.28	-0.41	-0.53
10	PS97/024-2	54° 35.27' S	73° 57.30' W	1272.8	-	-	-
11	PS97/022-1	54° 42.03' S	73° 48.38' W	1615.1	0.27	-0.41	-0.55
12	PS97/021-1	55° 6.91' S	72° 40.09' W	1840.4	0.30	-0.41	-0.54
13	PS97/020-1	55° 30.80' S	71° 38.22' W	2104.3	0.27	-0.42	-0.54
14	PS97/015-2	55° 43.89' S	70° 53.55' W	1886.3	0.31	-0.42	-0.55
15	PS97/094-1	57° 0.17' S	70° 58.32' W	3993.4	0.31	-0.39	-0.52
16	PS97/093-3	57° 29.92' S	70° 16.57' W	3782.2	0.36	-0.42	-0.54
17	PS97/097-1	57° 3.27' S	67° 4.00' W	2318.6	0.30	-0.42	-0.53
18	PS97/096-1	56° 4.53' S	66° 8.96' W	1620.7	0.31	-0.44	-0.55
19	PS97/095-1	56° 14.68' S	66° 14.95' W	1652.1	0.25	-0.43	-0.55
<i>Drake Passage Shackleton Fracture Zone</i>							
20	PS97/089-2	58° 13.60' S	62° 43.63' W	3431.9	0.18	-0.43	-0.56
21	PS97/086-2	58° 38.65' S	61° 23.82' W	2968.9	0.15	-0.45	-0.56

22	PS97/085-2	58° 21.28' S	62° 10.07' W	3090.7	0.16	-0.43	-0.55
23*	PS97/084-2	58° 52.14' S	60° 51.91' W	3617.4	0.10	-0.46	-0.58
24*	PS97/083-1	58° 59.65' S	60° 34.28' W	3756.3	0.12	-0.49	-0.60
25*	PS97/080-2	59° 40.49' S	59° 37.86' W	3112.7	0.12	-0.46	-0.56
26*	PS97/079-1	60° 8.55' S	58° 59.42' W	3539.3	0.07	-0.48	-0.61
<i>Drake Passage Phoenix Antarctic Ridge</i>							
27*	PS97/042-1	59° 50.62' S	66° 5.77' W	4172	0.12	-0.43	-0.54
28*	PS97/044-1	60° 36.80' S	66° 1.34' W	1202.8	-	-0.48	-0.57
29*	PS97/045-1	60° 34.27' S	66° 5.67' W	2292	0.14	-0.47	-0.55
30*	PS97/046-6	60° 59.74' S	65° 21.40' W	2802.7	0.13	-0.45	-0.56
31*	PS97/048-1	61° 26.40' S	64° 53.27' W	3455.2	0.14	-0.42	-0.55
32*	PS97/049-2	61° 40.28' S	64° 57.74' W	3752.2	0.14	-0.47	-0.58
33*	PS97/052-3	62° 29.93' S	64° 17.63' W	2889.8	-	-0.46	-0.60

674 * [isoGDGTs Lamping et al. \(2021\); Alkenone *this study*](#)

675

676 **Data availability.** All locations and the three main indices of the new 33 samples of this study are available in **Table A2**.

677

678 **Author contributions.** The study was conceived by JRH and LL-J; MEV, JRH, JH and NR contributed with analytical tools;
679 JRH, LL-J, JK, AJ analyzed data; JRH drafted the paper and figures; LL-J supervised the study. All authors contributed to the
680 interpretation and discussion of the results as well as commented on, or contributed to the draft and final version of the
681 manuscript.

682

683 **Acknowledgements.** We thank master and crew of R/V Polarstern, as well as the science party for their professional support
684 on expedition PS97 “Paleo-Drake”. We thank Sophie Ehrhardt for providing unpublished alkenone data. We thank the
685 technicians Walter Luttmer and Denise Diekstall for their support in the laboratory. We acknowledge funding through the
686 AWI institutional research programs “PACES-IP” and “Changing Earth – Sustaining our Future”, as well as through the
687 REKLIM initiative. [We acknowledge the use of imagery from the NASA Worldview application](#)
688 (<https://worldview.earthdata.nasa.gov/>), part of the NASA Earth Observing System Data and Information System (EOSDIS).

689

690

691 **Financial support.** This research has been supported by the AWI institutional research programs “PACE-IP” and “Changing
692 Earth – Sustaining our Future”, as well as through the REKLIM initiative.

693

694 **Competing Interests.** The authors declare no conflict of interest.

695

696 **References**

- 697 Basse, A., Zhu, C., Versteegh, G. J. M., Fischer, G., Hinrichs, K. U., and Mollenhauer, G.: Distribution of intact and core tetraether lipids in
698 water column profiles of suspended particulate matter off Cape Blanc, NW Africa, *Organic Geochemistry*, 72, 1-13,
699 10.1016/j.orggeochem.2014.04.007, 2014.
- 700 Baumann, K.-H., Andruleit, H., Böckel, B., Geisen, M., and Kinkel, H.: The significance of extant coccolithophores as indicators of ocean
701 water masses, surface water temperature, and palaeoproductivity: a review, *Paläontologische Zeitschrift*, 79, 93-112,
702 10.1007/bf03021756, 2005.
- 703 Belt, S. T., Brown, T. A., Ampel, L., Cabedo-Sanz, P., Fahl, K., Kocis, J. J., Massé, G., Navarro-Rodriguez, A., Ruan, J., and Xu, Y.: An
704 inter-laboratory investigation of the Arctic sea ice biomarker proxy IP₂₅ in marine sediments: key outcomes
705 and recommendations, *Climate of the Past*, 10, 155-166, 10.5194/cp-10-155-2014, 2014.
- 706 Brassell, S. C., Eglinton, G., Marlowe, I. T., Pflaumann, U., and Samthein, M.: Molecular Stratigraphy - a New Tool for Climatic
707 Assessment, *Nature*, 320, 129-133, 10.1038/320129a0, 1986.
- 708 Brochier-Armanet, C., Boussau, B., Gribaldo, S., and Forterre, P.: Mesophilic Crenarchaeota: proposal for a third archaeal phylum, the
709 Thaumarchaeota, *Nat Rev Microbiol*, 6, 245-252, 10.1038/nrmicro1852, 2008.
- 710 Burke, K. D., Williams, J. W., Chandler, M. A., Haywood, A. M., Lunt, D. J., and Otto-Bliesner, B. L.: Pliocene and Eocene provide best
711 analogs for near-future climates, *Proc Natl Acad Sci U S A*, 115, 13288-13293, 10.1073/pnas.1809600115, 2018.
- 712 Caniupán, M., Lamy, F., Lange, C. B., Kaiser, J., Kilian, R., Arz, H. W., León, T., Mollenhauer, G., Sandoval, S., De Pol-Holz, R., Pantoja,
713 S., Wellner, J., and Tiedemann, R.: Holocene sea-surface temperature variability in the Chilean fjord region, *Quaternary Research*,
714 82, 342-353, 10.1016/j.yqres.2014.07.009, 2014.
- 715 Chong, P. L.: Archaeobacterial bipolar tetraether lipids: Physico-chemical and membrane properties, *Chem Phys Lipids*, 163, 253-265,
716 10.1016/j.chemphyslip.2009.12.006, 2010.
- 717 Conte, M. H., Sicre, M.-A., Rühlemann, C., Weber, J. C., Schulte, S., Schulz-Bull, D., and Blanz, T.: Global temperature calibration of the
718 alkenone unsaturation index (UK'37) in surface waters and comparison with surface sediments, *Geochemistry, Geophysics,*
719 *Geosystems*, 7, 10.1029/2005gc001054, 2006.
- 720 D'Hondt, S., Spivack, A. J., Pockalny, R., Ferdelman, T. G., Fischer, J. P., Kallmeyer, J., Abrams, L. J., Smith, D. C., Graham, D., Hasiuk,
721 F., Schrum, H., and Stancin, A. M.: Subseafloor sedimentary life in the South Pacific Gyre, *Proc Natl Acad Sci U S A*, 106, 11651-
722 11656, 10.1073/pnas.0811793106, 2009.
- 723 Dávila, P. M., Figueroa, D., and Müller, E.: Freshwater input into the coastal ocean and its relation with the salinity distribution off austral
724 Chile (35–55°S), *Continental Shelf Research*, 22, 521-534, 10.1016/s0278-4343(01)00072-3, 2002.
- 725 Dong, L., Li, Z. Y., and Jia, G. D.: Archaeal ammonia oxidation plays a part in late Quaternary nitrogen cycling in the South China Sea,
726 *Earth and Planetary Science Letters*, 509, 38-46, 10.1016/j.epsl.2018.12.023, 2019.
- 727 Durak, G. M., Taylor, A. R., Walker, C. E., Probert, I., de Vargas, C., Audic, S., Schroeder, D., Brownlee, C., and Wheeler, G. L.: A role
728 for diatom-like silicon transporters in calcifying coccolithophores, *Nat Commun*, 7, 10543, 10.1038/ncomms10543, 2016.
- 729 Elling, F. J., Konneke, M., Mussmann, M., Greve, A., and Hinrichs, K. U.: Influence of temperature, pH, and salinity on membrane lipid
730 composition and TEX86 of marine planktonic thaumarchaeal isolates, *Geochimica Et Cosmochimica Acta*, 171, 238-255,
731 10.1016/j.gca.2015.09.004, 2015.
- 732 Epstein, B. L., D'Hondt, S., and Hargraves, P. E.: The possible metabolic role of C37 alkenones in *Emiliania huxleyi*, *Organic Geochemistry*,
733 32, 867-875, 10.1016/s0146-6380(01)00026-2, 2001.
- 734 Fietz, S., Ho, S. L., and Huguet, C.: Archaeal Membrane Lipid-Based Paleothermometry for Applications in Polar Oceans, *Oceanography*,
735 33, 104-114, 10.5670/oceanog.2020.207, 2020.
- 736 Fietz, S., Ho, S. L., Huguet, C., Rosell-Mele, A., and Martinez-Garcia, A.: Appraising GDGT-based seawater temperature indices in the
737 Southern Ocean, *Organic Geochemistry*, 102, 93-105, 10.1016/j.orggeochem.2016.10.003, 2016.
- 738 Fietz, S., Huguet, C., Rueda, G., Hambach, B., and Rosell-Mele, A.: Hydroxylated isoprenoidal GDGTs in the Nordic Seas, *Marine*
739 *Chemistry*, 152, 1-10, 10.1016/j.marchem.2013.02.007, 2013.
- 740 Gabriel, J. L. and Chong, P. L.: Molecular modeling of archaeobacterial bipolar tetraether lipid membranes, *Chem Phys Lipids*, 105, 193-
741 200, 10.1016/s0009-3084(00)00126-2, 2000.

742 Garreaud, R., Lopez, P., Minvielle, M., and Rojas, M.: Large-Scale Control on the Patagonian Climate, *Journal of Climate*, 26, 215-230,
743 10.1175/JCLI-D-12-00001.1, 2013.

744 Global Modeling and Assimilation Office (GAMO): MERRA-2 tavgM_2d_adg_Nx: 2d,Monthly mean,Time-averaged,Single-
745 Level,Assimilation,Aerosol Diagnostics (extended) V5.12.4 [dataset], 10.5067/RZIK2TV7PP38, 2015.

746 Herbert, T. D.: Review of alkenone calibrations (culture, water column, and sediments), *Geochemistry Geophysics Geosystems*, 2,
747 10.1029/2000gc000055, 2001.

748 Herbert, T. D.: Alkenone Paleotemperature Determinations, in: *Treatise on Geochemistry*, 399-433, 10.1016/b978-0-08-095975-7.00615-x,
749 2014.

750 Herbert, T. D., Peterson, L. C., Lawrence, K. T., and Liu, Z.: Tropical ocean temperatures over the past 3.5 million years, *Science*, 328,
751 1530-1534, 10.1126/science.1185435, 2010.

752 Hernández-Sánchez, M. T., Woodward, E. M. S., Taylor, K. W. R., Henderson, G. M., and Pancost, R. D.: Variations in GDGT distributions
753 through the water column in the South East Atlantic Ocean, *Geochimica et Cosmochimica Acta*, 132, 337-348,
754 10.1016/j.gca.2014.02.009, 2014.

755 Ho, S. L., Mollenhauer, G., Lamy, F., Martinez-Garcia, A., Mohtadi, M., Gersonde, R., Hebbeln, D., Nunez-Ricardo, S., Rosell-Mele, A.,
756 and Tiedemann, R.: Sea surface temperature variability in the Pacific sector of the Southern Ocean over the past 700 kyr,
757 *Paleoceanography*, 27, 10.1029/2012pa002317, 2012.

758 Ho, S. L., Mollenhauer, G., Fietz, S., Martinez-Garcia, A., Lamy, F., Rueda, G., Schipper, K., Meheust, M., Rosell-Mele, A., Stein, R., and
759 Tiedemann, R.: Appraisal of TEX86 and TEX86L thermometries in subpolar and polar regions, *Geochimica Et Cosmochimica Acta*,
760 131, 213-226, 10.1016/j.gca.2014.01.001, 2014.

761 Hopmans, E. C., Schouten, S., and Damste, J. S. S.: The effect of improved chromatography on GDGT-based palaeoproxies, *Organic*
762 *Geochemistry*, 93, 1-6, 10.1016/j.orggeochem.2015.12.006, 2016.

763 Hopmans, E. C., Weijers, J. W. H., Schefuss, E., Herfort, L., Damste, J. S. S., and Schouten, S.: A novel proxy for terrestrial organic matter
764 in sediments based on branched and isoprenoid tetraether lipids, *Earth and Planetary Science Letters*, 224, 107-116,
765 10.1016/j.epsl.2004.05.012, 2004.

766 Huguet, C., Fietz, S., and Rosell-Mele, A.: Global distribution patterns of hydroxy glycerol dialkyl glycerol tetraethers, *Organic*
767 *Geochemistry*, 57, 107-118, 10.1016/j.orggeochem.2013.01.010, 2013.

768 Jaeschke, A., Wengler, M., Hefter, J., Ronge, T. A., Geibert, W., Mollenhauer, G., Gersonde, R., and Lamy, F.: A biomarker perspective on
769 dust, productivity, and sea surface temperature in the Pacific sector of the Southern Ocean, *Geochimica Et Cosmochimica Acta*, 204,
770 120-139, 10.1016/j.gca.2017.01.045, 2017.

771 Kaiser, J., Schouten, S., Kilian, R., Arz, H. W., Lamy, F., and Damste, J. S. S.: Isoprenoid and branched GDGT-based proxies for surface
772 sediments from marine, fjord and lake environments in Chile, *Organic Geochemistry*, 89-90, 117-127,
773 10.1016/j.orggeochem.2015.10.007, 2015.

774 Kalanetra, K. M., Bano, N., and Hollibaugh, J. T.: Ammonia-oxidizing Archaea in the Arctic Ocean and Antarctic coastal waters, *Environ*
775 *Microbiol*, 11, 2434-2445, 10.1111/j.1462-2920.2009.01974.x, 2009.

776 Karner, M. B., DeLong, E. F., and Karl, D. M.: Archaeal dominance in the mesopelagic zone of the Pacific Ocean, *Nature*, 409, 507-510,
777 10.1038/35054051, 2001.

778 Kim, J. H., Villanueva, L., Zell, C., and Damste, J. S. S.: Biological source and provenance of deep-water derived isoprenoid tetraether lipids
779 along the Portuguese continental margin, *Geochimica Et Cosmochimica Acta*, 172, 177-204, 10.1016/j.gca.2015.09.010, 2016.

780 Kim, J. H., Romero, O. E., Lohmann, G., Donner, B., Laepple, T., Haam, E., and Damste, J. S. S.: Pronounced subsurface cooling of North
781 Atlantic waters off Northwest Africa during Dansgaard-Oeschger interstadials, *Earth and Planetary Science Letters*, 339, 95-102,
782 10.1016/j.epsl.2012.05.018, 2012a.

783 Kim, J. H., Crosta, X., Willmott, V., Renssen, H., Bonnín, J., Helmke, P., Schouten, S., and Damste, J. S. S.: Holocene subsurface temperature
784 variability in the eastern Antarctic continental margin, *Geophysical Research Letters*, 39, 10.1029/2012gl051157, 2012b.

785 Kim, J. H., van der Meer, J., Schouten, S., Helmke, P., Willmott, V., Sangiorgi, F., Koc, N., Hopmans, E. C., and Damste, J. S. S.: New
786 indices and calibrations derived from the distribution of crenarchaeal isoprenoid tetraether lipids: Implications for past sea surface
787 temperature reconstructions, *Geochimica Et Cosmochimica Acta*, 74, 4639-4654, 10.1016/j.gca.2010.05.027, 2010.

788 Kim, J. H., Schouten, S., Rodrigo-Gamiz, M., Rampen, S., Marino, G., Huguet, C., Helmke, P., Buscail, R., Hopmans, E. C., Pross, J.,
789 Sangiorgi, F., Middelburg, J. B. M., and Damste, J. S. S.: Influence of deep-water derived isoprenoid tetraether lipids on the TEX86H
790 paleothermometer in the Mediterranean Sea, *Geochimica Et Cosmochimica Acta*, 150, 125-141, 10.1016/j.gca.2014.11.017, 2015.

791 Koenig, Z., Provost, C., Ferrari, R., Sennechaël, N., and Rio, M. H.: Volume transport of the Antarctic Circumpolar Current: Production and
792 validation of a 20 year long time series obtained from in situ and satellite observations, *Journal of Geophysical Research-Oceans*,
793 119, 5407-5433, 10.1002/2014jc009966, 2014.

794 Lamping, N., Muller, J., Hefter, J., Mollenhauer, G., Haas, C., Shi, X. X., Vorrath, M. E., Lohmann, G., and Hillenbrand, C. D.: Evaluation
795 of lipid biomarkers as proxies for sea ice and ocean temperatures along the Antarctic continental margin, *Climate of the Past*, 17,
796 2305-2326, 10.5194/cp-17-2305-2021, 2021.

797 Lamy, F.: The Expedition PS97 of the Research Vessel POLARSTERN to the Drake Passage in 2016 , Berichte zur Polar- und
798 Meeresforschung = Reports on polar and marine research, Bremerhaven, Alfred Wegener Institute for Polar and Marine Research,
799 571 p., http://doi.org/10.2312/BzPM_0701_2016, 2016.

800 Lamy, F., Kilian, R., Arz, H. W., Francois, J. P., Kaiser, J., Prange, M., and Steinke, T.: Holocene changes in the position and intensity of
801 the southern westerly wind belt, *Nature Geoscience*, 3, 695-699, 10.1038/Ngeo959, 2010.

802 Lamy, F., Gersonde, R., Winckler, G., Esper, O., Jaeschke, A., Kuhn, G., Ullermann, J., Martinez-Garcia, A., Lambert, F., and Kilian, R.:
803 Increased dust deposition in the Pacific Southern Ocean during glacial periods, *Science*, 343, 403-407, 10.1126/science.1245424,
804 2014.

805 Liu, R. J., Han, Z. B., Zhao, J., Zhang, H. F., Li, D., Ren, J. Y., Pan, J. M., and Zhang, H. S.: Distribution and source of glycerol dialkyl
806 glycerol tetraethers (GDGTs) and the applicability of GDGT-based temperature proxies in surface sediments of Prydz Bay, East
807 Antarctica, *Polar Research*, 39, 10.33265/polar.v39.3557, 2020.

808 Locarnini, R. A., Mishonov, A. V., Antonov, J. I., Boyer, T. P., and Garcia, H. E.: World Ocean Atlas 2005, Volume 1: Temperature, S.
809 Levitus, Ed. NOAA Atlas NESDIS 61 [dataset], 2006.

810 Locarnini, R. A., Mishonov, A. V., Antonov, J. I., Boyer, T. P., Garcia, H. E., Baranova, O. K., Zweng, M. M., and Johnson, D. R.: World
811 Ocean Atlas 2009, Volume 1: Temperature S. Levitus, Ed., NOAA Atlas NESDIS 68, U.S. Government Printing Office,
812 Washington, D.C., 184 pp., 2010.

813 Lü, X., Liu, X.-L., Elling, F. J., Yang, H., Xie, S., Song, J., Li, X., Yuan, H., Li, N., and Hinrichs, K.-U.: Hydroxylated isoprenoid GDGTs
814 in Chinese coastal seas and their potential as a paleotemperature proxy for mid-to-low latitude marginal seas, *Organic Geochemistry*,
815 89-90, 31-43, 10.1016/j.orggeochem.2015.10.004, 2015.

816 Massana, R., Taylor, L. J., Murray, A. E., Wu, K. Y., Jeffrey, W. H., and DeLong, E. F.: Vertical distribution and temporal variation of
817 marine planktonic archaea in the Gerlache Strait, Antarctica, during early spring, *Limnology and Oceanography*, 43, 607-617,
818 10.4319/lo.1998.43.4.0607, 1998.

819 Max, L., Lembke-Jene, L., Zou, J., Shi, X., and Tiedemann, R.: Evaluation of reconstructed sea surface temperatures based on U37k' from
820 sediment surface samples of the North Pacific, *Quaternary Science Reviews*, 243, 10.1016/j.quascirev.2020.106496, 2020.

821 Méheust, M., Fahl, K., and Stein, R.: Variability in modern sea surface temperature, sea ice and terrigenous input in the sub-polar North
822 Pacific and Bering Sea: Reconstruction from biomarker data, *Organic Geochemistry*, 57, 54-64, 10.1016/j.orggeochem.2013.01.008,
823 2013.

824 Müller, P. J., Kirst, G., Ruhland, G., von Storch, I., and Rosell-Melé, A.: Calibration of the alkenone paleotemperature index U37K' based
825 on core-tops from the eastern South Atlantic and the global ocean (60°N-60°S), *Geochimica et Cosmochimica Acta*, 62, 1757-1772,
826 10.1016/s0016-7037(98)00097-0, 1998.

827 Murray, A. E., Preston, C. M., Massana, R., Taylor, L. T., Blakis, A., Wu, K., and DeLong, E. F.: Seasonal and spatial variability of bacterial
828 and archaeal assemblages in the coastal waters near Anvers Island, Antarctica, *Appl Environ Microbiol*, 64, 2585-2595,
829 10.1128/AEM.64.7.2585-2595.1998, 1998.

830 Orsi, A. H., Whitworth, T., and Nowlin, W. D.: On the Meridional Extent and Fronts of the Antarctic Circumpolar Current, *Deep-Sea*
831 *Research Part I-Oceanographic Research Papers*, 42, 641-673, 10.1016/0967-0637(95)00021-W, 1995.

832 Pearson, A. and Ingalls, A. E.: Assessing the Use of Archaeal Lipids as Marine Environmental Proxies, *Annual Review of Earth and*
833 *Planetary Sciences*, Vol 41, 41, 359-384, 10.1146/annurev-earth-050212-123947, 2013.

834 Popp, B. N., Kenig, F., Wakeham, S. G., Laws, E. A., and Bidigare, R. R.: Does growth rate affect ketone unsaturation and intracellular
835 carbon isotopic variability in *Emiliania huxleyi*?, *Paleoceanography*, 13, 35-41, 10.1029/97pa02594, 1998.

836 Prahl, F. G. and Wakeham, S. G.: Calibration of unsaturation patterns in long-chain ketone compositions for palaeotemperature assessment,
837 *Nature*, 330, 367-369, 10.1038/330367a0, 1987.

838 Prahl, F. G., Mix, A. C., and Sparrow, M. A.: Alkenone paleothermometry: Biological lessons from marine sediment records off western
839 South America, *Geochimica Et Cosmochimica Acta*, 70, 101-117, 10.1016/j.gca.2005.08.023, 2006.

840 Prahl, F. G., Muehlhausen, L. A., and Zahnle, D. L.: Further Evaluation of Long-Chain Alkenones as Indicators of Paleoceanographic
841 Conditions, *Geochimica Et Cosmochimica Acta*, 52, 2303-2310, 10.1016/0016-7037(88)90132-9, 1988.

842 Prahl, F. G., Rontani, J. F., Zabeti, N., Walinsky, S. E., and Sparrow, M. A.: Systematic pattern in U-37(K') - Temperature residuals for
843 surface sediments from high latitude and other oceanographic settings, *Geochimica Et Cosmochimica Acta*, 74, 131-143,
844 10.1016/j.gca.2009.09.027, 2010.

845 Qin, W., Carlson, L. T., Armbrust, E. V., Devol, A. H., Moffett, J. W., Stahl, D. A., and Ingalls, A. E.: Confounding effects of oxygen and
846 temperature on the TEX86 signature of marine Thaumarchaeota, *Proc Natl Acad Sci U S A*, 112, 10979-10984,
847 10.1073/pnas.1501568112, 2015.

848 Quiñones, R. A., Levipan, H. A., and Urrutia, H.: Spatial and temporal variability of planktonic archaeal abundance in the Humboldt Current
849 System off Chile, *Deep Sea Research Part II: Topical Studies in Oceanography*, 56, 1073-1082, 10.1016/j.dsr2.2008.09.012, 2009.

850 Rintoul, S. R.: The global influence of localized dynamics in the Southern Ocean, *Nature*, 558, 209-218, 10.1038/s41586-018-0182-3, 2018.

851 Saavedra-Pellitero, M., Baumann, K. H., Flores, J. A., and Gersonde, R.: Biogeographic distribution of living coccolithophores in the Pacific
852 sector of the Southern Ocean, *Marine Micropaleontology*, 109, 1-20, 10.1016/j.marmicro.2014.03.003, 2014.

853 Saavedra-Pellitero, M., Baumann, K. H., Fuertes, M. A., Schulz, H., Marcon, Y., Vollmar, N. M., Flores, J. A., and Lamy, F.: Calcification
854 and latitudinal distribution of extant coccolithophores across the Drake Passage during late austral summer 2016, *Biogeosciences*,
855 16, 3679-3702, 10.5194/bg-16-3679-2019, 2019.

856 Schneider, C., Glaser, M., Kilian, R., Santana, A., Butorovic, N., and Casassa, G.: Weather Observations Across the Southern Andes at 53°S,
857 *Physical Geography*, 24, 97-119, 10.2747/0272-3646.24.2.97, 2003.

858 Schouten, S., Hopmans, E. C., and Damste, J. S. S.: The organic geochemistry of glycerol dialkyl glycerol tetraether lipids: A review,
859 *Organic Geochemistry*, 54, 19-61, 10.1016/j.orggeochem.2012.09.006, 2013a.

860 Schouten, S., Hopmans, E. C., Schefuß, E., and Sinninghe Damsté, J. S.: Distributional variations in marine crenarchaeotal membrane lipids:
861 a new tool for reconstructing ancient sea water temperatures?, *Earth and Planetary Science Letters*, 204, 265-274, 10.1016/s0012-
862 821x(02)00979-2, 2002.

863 Schouten, S., Huguet, C., Hopmans, E. C., Kienhuis, M. V., and Damste, J. S. S.: Analytical methodology for TEX86 paleothermometry by
864 high-performance liquid chromatography/atmospheric pressure chemical ionization-mass spectrometry, *Anal Chem*, 79, 2940-2944,
865 10.1021/ac062339v, 2007.

866 Schouten, S., Pitcher, A., Hopmans, E. C., Villanueva, L., van Bleijswijk, J., and Damste, J. S. S.: Intact polar and core glycerol dibiphytanyl
867 glycerol tetraether lipids in the Arabian Sea oxygen minimum zone: I. Selective preservation and degradation in the water column
868 and consequences for the TEX86, *Geochimica Et Cosmochimica Acta*, 98, 228-243, 10.1016/j.gca.2012.05.002, 2012.

869 Schouten, S., Hopmans, E. C., Rosell-Melé, A., Pearson, A., Adam, P., Bauersachs, T., Bard, E., Bernasconi, S. M., Bianchi, T. S., Brooks,
870 J. J., Carlson, L. T., Castañeda, I. S., Derenne, S., Selver, A. D., Dutta, K., Eglinton, T., Fosse, C., Galy, V., Grice, K., Hinrichs, K.-
871 U., Huang, Y., Huguet, A., Huguet, C., Hurley, S., Ingalls, A., Jia, G., Keely, B., Knappy, C., Kondo, M., Krishnan, S., Lincoln, S.,
872 Lipp, J., Mangelsdorf, K., Martínez-García, A., Ménot, G., Mets, A., Mollenhauer, G., Ohkouchi, N., Ossebaar, J., Pagani, M.,
873 Pancost, R. D., Pearson, E. J., Peterse, F., Reichart, G.-J., Schaeffer, P., Schmitt, G., Schwark, L., Shah, S. R., Smith, R. W.,
874 Smittenberg, R. H., Summons, R. E., Takano, Y., Talbot, H. M., Taylor, K. W. R., Tarozo, R., Uchida, M., van Dongen, B. E., Van
875 Mooy, B. A. S., Wang, J., Warren, C., Weijers, J. W. H., Wernke, J. P., Woltering, M., Xie, S., Yamamoto, M., Yang, H., Zhang, C.
876 L., Zhang, Y., Zhao, M., and Damsté, J. S. S.: An interlaboratory study of TEX86 and BIT analysis of sediments, extracts, and
877 standard mixtures, *Geochemistry, Geophysics, Geosystems*, 14, 5263-5285, 10.1002/2013gc004904, 2013b.

878 Sikes, E. L., Volkman, J. K., Robertson, L. G., and Pichon, J. J.: Alkenones and alkenes in surface waters and sediments of the Southern
879 Ocean: Implications for paleotemperature estimation in polar regions, *Geochimica Et Cosmochimica Acta*, 61, 1495-1505,
880 10.1016/S0016-7037(97)00017-3, 1997.

881 Smith, H. E. K., Poulton, A. J., Garley, R., Hopkins, J., Lubelczyk, L. C., Drapeau, D. T., Rauschenberg, S., Twining, B., Bates, N. R., and
882 Balch, W. M.: The influence of environmental variability on the biogeography of coccolithophores and diatoms in the Great Calcite
883 Belt, *Biogeosciences*, 14, 4905-4925, 10.5194/bg-14-4905-2017, 2017.

884 Strub, P. T., Mesías, J. M., Montecino, V., Rutllant, J., and Salinas, S.: Chapter 10. Coastal ocean circulation off western south america
885 coastal segment, in: *The Sea*, edited by: Robinson, A. R., and Kennen, H. B., 273-313, 1998.

886 Taylor, K. W. R., Huber, M., Hollis, C. J., Hernandez-Sanchez, M. T., and Pancost, R. D.: Re-evaluating modern and Palaeogene GDGT
887 distributions: Implications for SST reconstructions, *Global and Planetary Change*, 108, 158-174, 10.1016/j.gloplacha.2013.06.011,
888 2013.

889 Toyos, M. H., Winckler, G., Arz, H. W., Lembke-Jene, L., Lange, C. B., Kuhn, G., and Lamy, F.: Variations in export production, lithogenic
890 sediment transport and iron fertilization in the Pacific sector of the Drake Passage over the past 400 kyr, *Climate of the Past*, 18,
891 147-166, 10.5194/cp-18-147-2022, 2022.

892 Tyrrell, T. and Merico, A.: *Emiliania huxleyi*: bloom observations and the conditions that induce them, in: *Coccolithophores*, 75-97,
893 10.1007/978-3-662-06278-4_4, 2004.

894 Villanueva, L., Schouten, S., and Sinninghe Damsté, J. S.: Depth-related distribution of a key gene of the tetraether lipid biosynthetic pathway
895 in marine Thaumarchaeota, *Environ Microbiol*, 17, 3527-3539, 10.1111/1462-2920.12508, 2015.

896 Volkman, J. K.: Ecological and environmental factors affecting alkenone distributions in seawater and sediments, *Geochemistry Geophysics*
897 *Geosystems*, 1, n/a-n/a, 10.1029/2000gc000061, 2000.

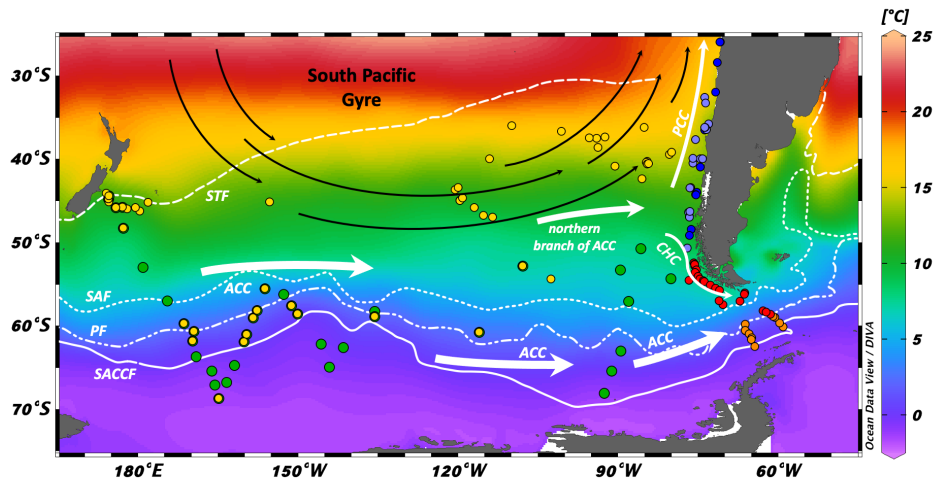
898 Vollmar, N. M., Baumann, K. H., Saavedra-Pellitero, M., and Hernandez-Almeida, I.: Distribution of coccoliths in surface sediments across
899 the Drake Passage and calcification of *Emiliania huxleyi* morphotypes, *Biogeosciences*, 19, 585-612, 10.5194/bg-19-585-2022,
900 2022.

901 Vorrath, M. E., Muller, J., Rebolledo, L., Cardenas, P., Shi, X. X., Esper, O., Opel, T., Geibert, W., Munoz, P., Haas, C., Kuhn, G., Lange,
902 C. B., Lohmann, G., and Mollenhauer, G.: Sea ice dynamics in the Bransfield Strait, Antarctic Peninsula, during past 240 years: a
903 multi-proxy intercomparison study, *Climate of the Past*, 16, 2459-2483, 10.5194/cp-16-2459-2020, 2020.

904 Watson, A. J., Vallis, G. K., and Nikurashin, M.: Southern Ocean buoyancy forcing of ocean ventilation and glacial atmospheric CO₂,
905 *Nature Geoscience*, 8, 10.1038/Ngeo2538, 2015.

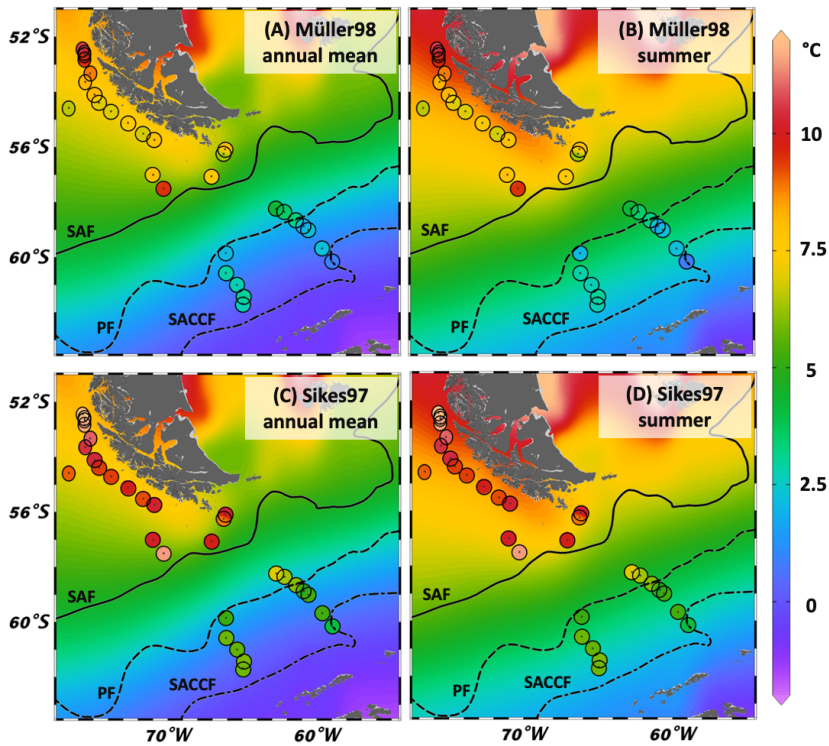
906 Weijers, J. W. H., Schouten, S., Spaargaren, O. C., and Damste, J. S. S.: Occurrence and distribution of tetraether membrane lipids in soils:
907 Implications for the use of the TEX86 proxy and the BIT index, *Organic Geochemistry*, 37, 1680-1693,
908 10.1016/j.orggeochem.2006.07.018, 2006.

909 Wuchter, C., Schouten, S., Wakeham, S. G., and Sinninghe Damsté, J. S.: Temporal and spatial variation in tetraether membrane lipids of
910 marine Crenarchaeota in particulate organic matter: Implications for TEX₈₆ paleothermometry, *Paleoceanography*, 20,
911 10.1029/2004pa001110, 2005.
912



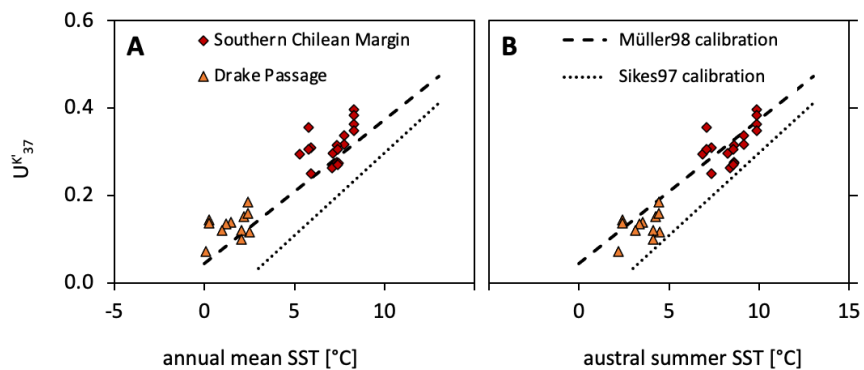
913
 914 Figure 1: Map with SSTs (WOA05; Locarnini et al., 2006) of the extended study area and sample locations. ACC: Antarctic
 915 Circumpolar Current; PCC: Peru-Chile Current; CHC: Cape Horn Current; STF: Subtropical Front; SAF: Subantarctic Front;
 916 PF: Polar Front; SACCF: Southern ACC Front. Red dots: Southern Chilean Margin and Drake Passage samples (this study);
 917 Orange dots: Drake Passage samples (Lamping et al., 2021; this study); Light blue dots: Northern – Central Chilean Margin samples
 918 (PrahI et al., 2006; PrahI et al., 2010); Dark blue dots: Northern – Central Chilean Margin samples (Kaiser et al., 2015); Yellow dots:
 919 South Pacific Gyre, Central South Pacific and New Zealand Margin samples (Jaeschke et al., 2017); Green dots: Central South
 920 Pacific and New Zealand Margin samples (Ho et al., 2014).

921



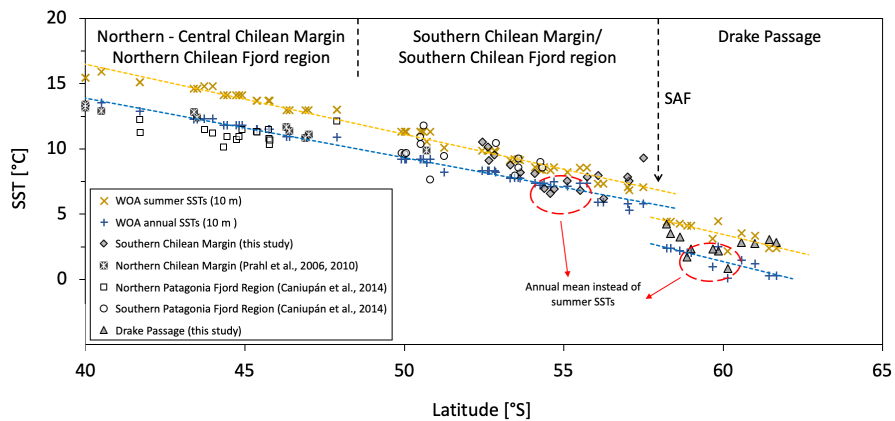
922
 923 Figure 2: Map of reconstructed SST values for $U^{K_{37}}$ (this study). Background gridded temperatures: WOA05 data (WOA05;
 924 Locarnini et al., 2006), colored dots are calculated SSTs. (A) WOA05 annual mean SSTs with Müller98 calibration; (B) WOA05
 925 summer SSTs with Müller98 calibration; (C) WOA05 annual mean SSTs with Sikes97 calibration; (D) WOA05 summer SSTs with
 926 Sikes97 calibration.

927

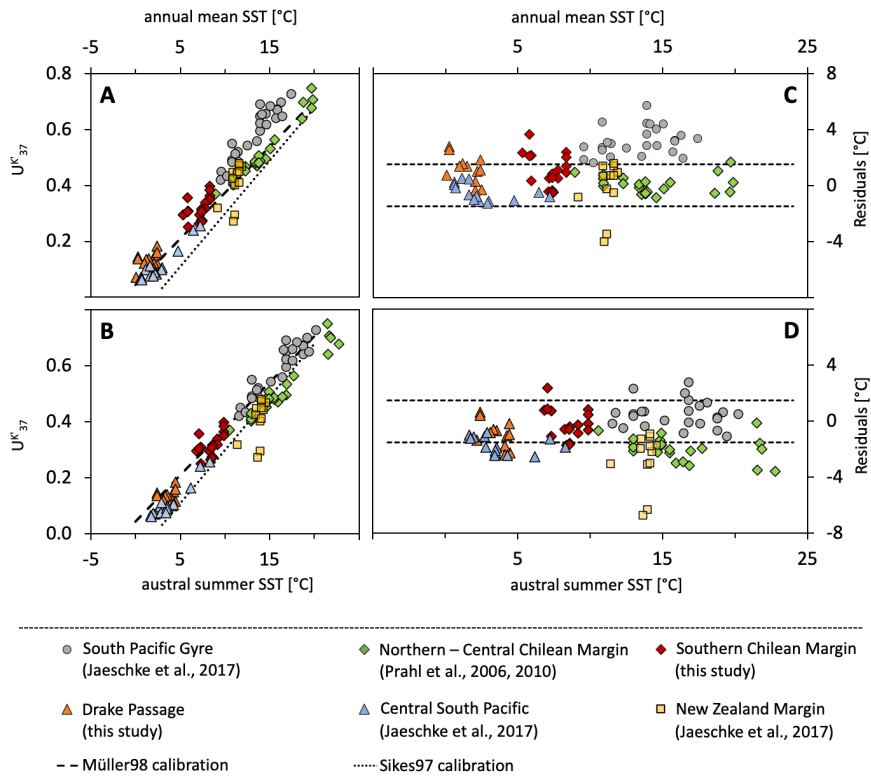


928
 929 **Figure 3: Comparison of $U^{K_{37}}$ index (this study) with modern SSTs at 10 m water depth (WOA05; Locarnini et al., 2006), for (A)**
 930 **annual mean SSTs, and (B) austral summer SSTs, corresponding to January – March.**

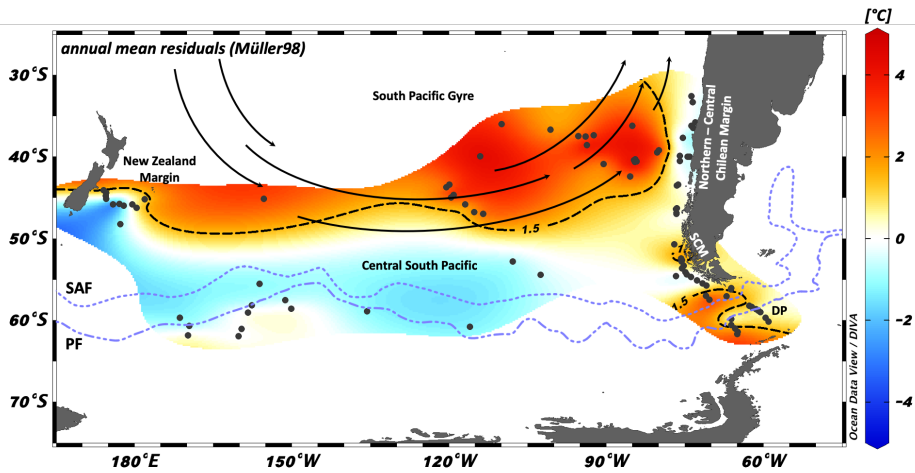
931



932
 933 **Figure 4: Comparison of ocean and fjord samples in the Chilean region. Yellow and Blue dashed lines show the meridional**
 934 **temperature evolution during summer and annual mean at 10 m water depth, respectively. Annual mean and summer data were**
 935 **taken from WOA09 (Locarnini et al., 2010) for the samples of Caniupán et al. (2014) and WOA05 (Locarnini et al., 2006) for Prah**
 936 **et al. (2006, 2010) and this study.**

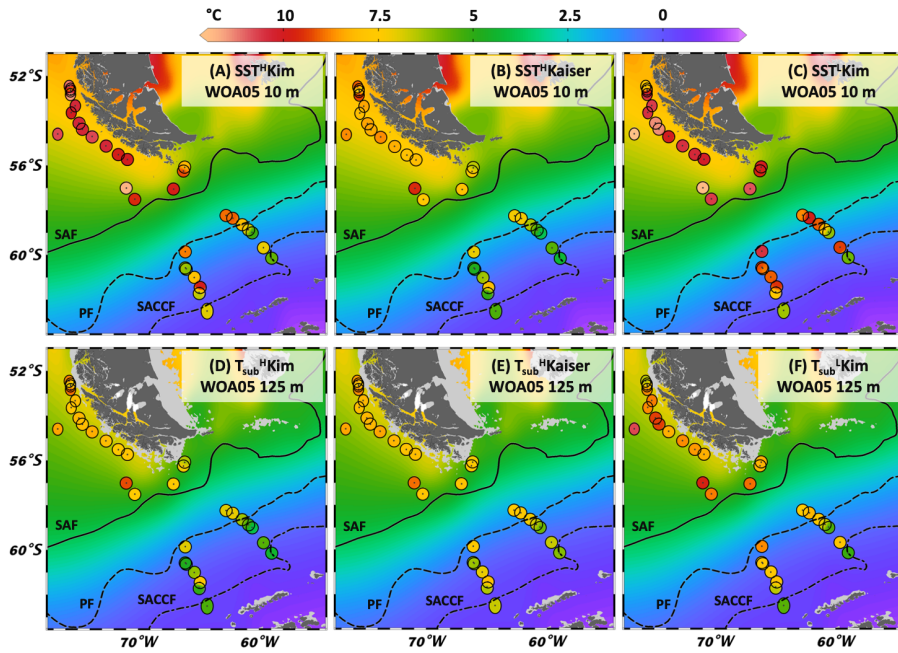


938
 939 **Figure 5:** (A) and (B): Compilation of $U^{K_{37}}$ index of this study and the expanded South Pacific study area with SSTs at 10 m water
 940 depth for annual mean and austral summer, respectively (WOA05; Locarnini et al., 2006). (C) and (D): Residuals of the local SSTs
 941 at 10 m water depth for the annual mean and austral summer (WOA05; Locarnini et al., 2006) subtracted by the Müller98 calculated
 942 SSTs. Temperature range of dotted line shows the standard error of the temperature calibration of $\pm 1.5^\circ \text{C}$ by Müller et al. (1998).
 943 Site PS75/088-6 (Jaeschke et al., 2017) was excluded due to unrealistic high temperatures of $>10^\circ \text{C}$.



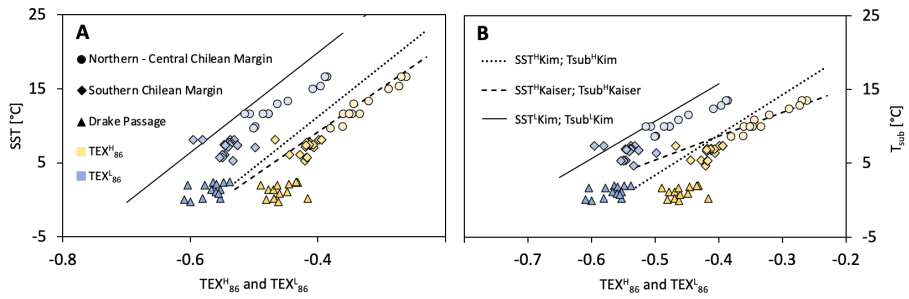
945
 946 Figure 6: Map with residuals for the extended study area of the South Pacific with published data from the Central South Pacific,
 947 the New Zealand Margin, the South Pacific Gyre (Jaeschke et al., 2017) and the Chilean Margin (Prahl et al., 2006; this study; Prahl
 948 et al., 2010). Atlas-derived annual mean WOA05 water temperatures of 10 m water depth (Locarnini et al., 2006) were subtracted
 949 from the SST Müller98 calibration. SCM: Southern Chilean Margin; DP: Drake Passage; SAF: Subantarctic Front; PF: Polar
 950 Front.

951



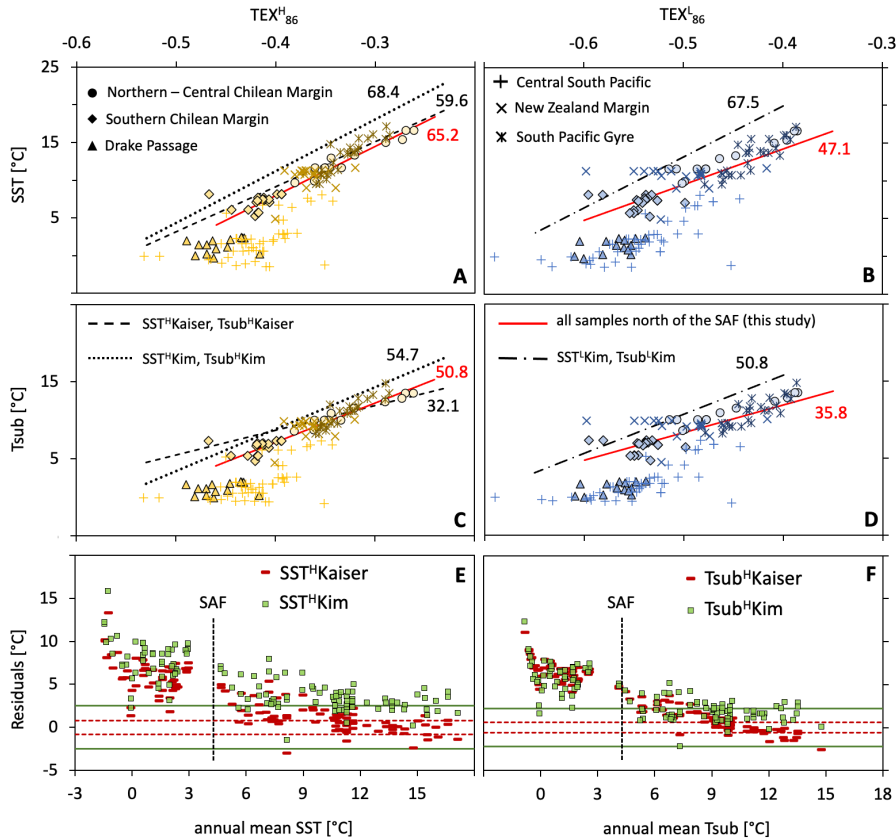
952
 953 Figure 7: Map of reconstructed SST and Tsub values for $\text{TEX}_{86}^{\text{H}}$ and $\text{TEX}_{86}^{\text{L}}$ (this study). Background gridded annual mean
 954 temperatures at 10 or 125 m water depth: WOA05 data, colored dots are calculated SSTs or Tsub. (A) WOA05 SSTs with calculated
 955 data after $\text{SST}^{\text{H}}\text{Kim}$; (B) WOA05 SSTs with calculated data after $\text{SST}^{\text{H}}\text{Kaiser}$; (C) WOA05 SSTs with calculated data after
 956 $\text{SST}^{\text{L}}\text{Kim}$; (D) WOA05 Tsub with calculated data after $\text{Tsub}^{\text{H}}\text{Kim}$; (E) WOA05 Tsub with calculated data after $\text{Tsub}^{\text{H}}\text{Kaiser}$; (F)
 957 WOA05 Tsub with calculated data after $\text{Tsub}^{\text{L}}\text{Kim}$.

958



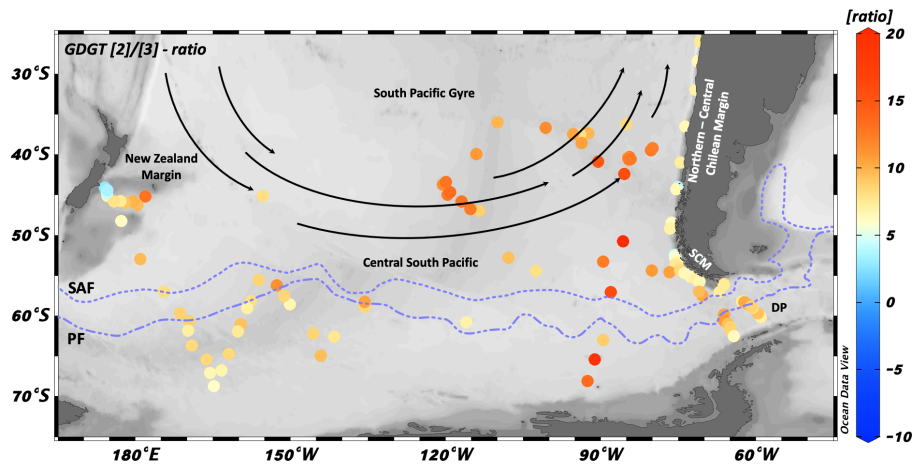
959
 960 **Figure 8:** Comparison of TEX₈₆^L (blue) and TEX₈₆^H (yellow) data with water temperature with the SST 0 – 50 m water depth and
 961 Tsub 0 – 200 m (WOA05; Locarnini et al., 2006), respectively. Black line: TEX₈₆ calibration line (SST^L-Kim, Tsub^L-Kim) for surface
 962 and subsurface, respectively. Circles: Kaiser et al. (2015); Route: this study; triangle: Lamping et al. (2021) and this study.

963



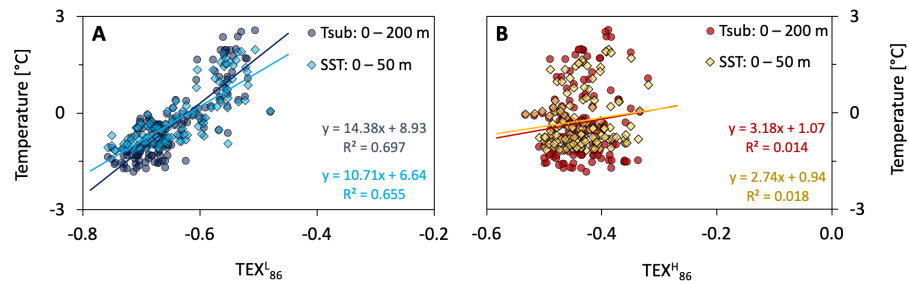
964
 965 Figure 9: (A) – (D): Comparison of TEX_{86}^H (yellow) and TEX_{86}^L (blue) data with annual mean water temperature with the SST 0 –
 966 50 m water depth and Tsub 0 – 200 m (WOA05; Locarnini et al., 2006), respectively. The black (previous studies) and red numbers
 967 (this study) indicate the slope of the corresponding calibration. Central South Pacific, New Zealand Margin and South Pacific Gyre
 968 samples: Ho et al. (2014) and Jaeschke et al. (2017); Northern – Central Chilean Margin samples: Kaiser et al. (2015); Southern
 969 Chilean Margin and Drake Passage samples: Lamping et al. (2021) and this study. (E) – (F): Residuals for SST 0 – 50 m and Tsub 0
 970 – 200 m, with modern world ocean atlas-based temperatures (WOA05; Locarnini et al., 2006) subtracted from the calibrated
 971 temperatures. Green solid lines: standard error of $\pm 2.5^\circ\text{C}$ (SST^HKim) and $\pm 2.2^\circ\text{C}$ (Tsub^HKim). Red dashed lines: Calibration
 972 standard errors of $\pm 0.8^\circ\text{C}$ (SST^HKaiser) and $\pm 0.6^\circ\text{C}$ (Tsub^HKaiser).

973



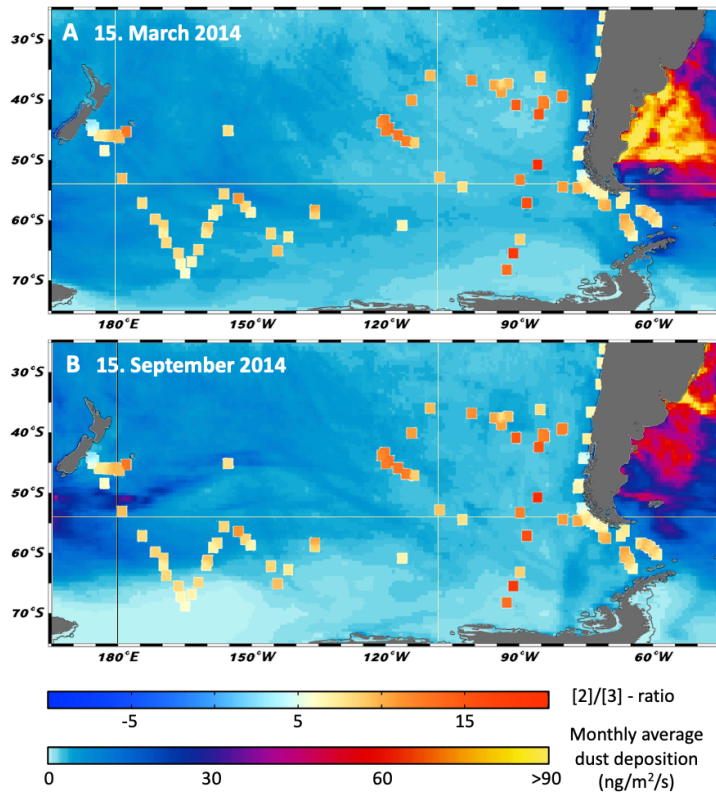
974
 975 Figure 10: Map of GDGT [2]/[3]-ratios from our extended surface sediment sample set across different regions within the study
 976 area. SCM: Southern Chilean Margin; DP: Drake Passage; SAF: Subantarctic Front; PF: Polar Front.

977



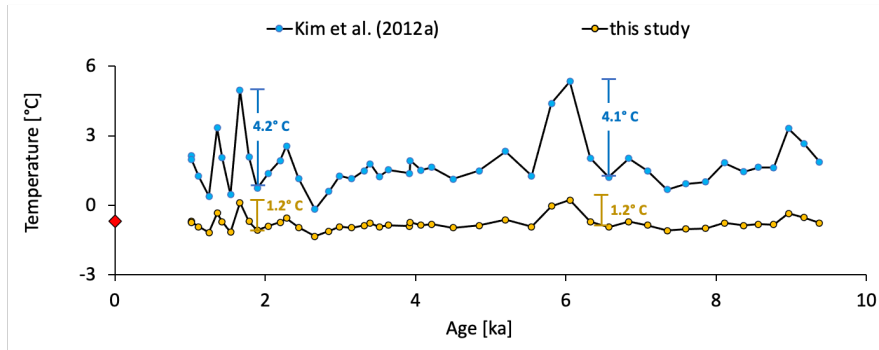
978
 979 Figure 11: TEX^H₈₆ and TEX^L₈₆ Indices south of the SAF vs. modern WOA05 water temperatures. (A) TEX^L₈₆ of all South Pacific
 980 samples; (B) TEX^H₈₆ of all South Pacific samples.

981



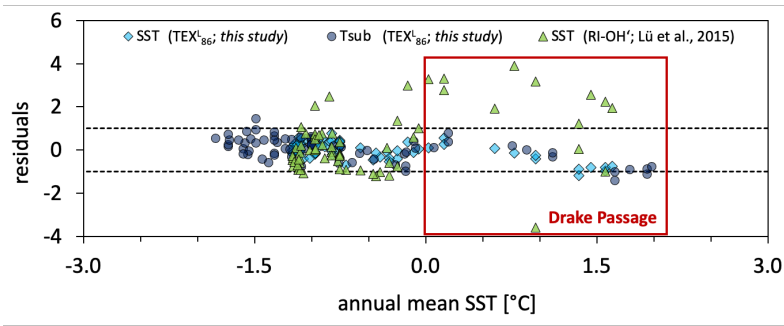
982
 983 **Figure 12:** GDOT [2]/[3]-ratio on a map, showing total monthly average dust deposition (dry + wet) for the times (A) march 2014
 984 and (B) September 2014. Dust data were taken from NASA worldview (Global Modeling and Assimilation Office (Gamo), 2015).

985



986
 987 **Figure 13:** Comparison of core MD03-2601 (Kim et al., 2012b) with the temperature calibration T_{sub}^L -Kim (blue) and the new
 988 subsurface calibration of this study (yellow). Red dot marked the mean temperature of 0 – 200 m water depth at the coring site.

989



990
 991 **Figure 14:** Residuals for SST 0 – 50 m and T_{sub} 0 – 200 m, with modern world ocean atlas-based temperatures (WOA05; Locarnini
 992 et al., 2006) subtracted from the calibrated temperatures. Black dashed lines mark the 1° C and -1° C isotherm, respectively.

993